

A Monte Carlo algorithm for spin foam intertwiners

Sebastian Steinhaus^a

^a *Theoretisch-Physikalisches Institut, Friedrich-Schiller-Universität Jena
Max-Wien-Platz 1, 07743 Jena, Germany, EU*

E-mail: sebastian.steinhaus@uni-jena.de

ABSTRACT: Monte Carlo algorithms are barely considered in spin foam quantum gravity. Due to the quantum nature of spin foam amplitudes one cannot readily apply them, and the present sign problem is a threat to convergence and thus efficiency. Yet, ultimately the severity of the sign problem in spin foams is not known. In this article we propose a new probability distribution for coherent (boundary) intertwiners, which we use to define a Markov Chain Monte Carlo algorithm. We apply this algorithm to the $SU(2)$ coherent vertex amplitude for various Regge-type boundary data and find convergent, accurate results at far lower costs than the explicit calculation. The resources are instead used to increase the size of boundary spins, bridging the gap to the asymptotic formulae. While the sign problem is not solved, it is under control in the vast majority of cases. We close by discussing how this algorithm can be extended to larger triangulations with boundary and 4d Lorentzian spin foam models. More speculatively, we discuss how this algorithm can be used to sample (Regge-geometric) bulk intertwiners.

Contents

1	Introduction	1
2	Spin Foam numerics and coherent amplitudes	5
2.1	Coherent $SU(2)$ vertex amplitude	7
3	Monte Carlo and the sign problem	9
3.1	Complex amplitudes and the sign problem	10
3.2	Probability distribution from coherent intertwiners	11
4	Approximating coherent vertex amplitudes	14
4.1	Sign problem in the coherent vertex amplitude	16
4.2	Results	17
4.3	Computational time	25
5	Discussion and conclusion	27
5.1	Generalizing the algorithm	29

1 Introduction

Spin foam quantum gravity [1, 2] is a non-perturbative, background independent path integral approach of quantum gravity, which is often referred to as a covariant formulation of loop quantum gravity [3, 4]. It constructs quantum space-time by gluing and superimposing quantum geometric building blocks [5]. These building blocks and their associated amplitudes are derived from general relativity written as a constrained topological quantum field theory [6, 7]. To regularize the path integral, the theory is discretised on a 2-complex, which is typically chosen to be dual to a triangulation, and then colored with group theoretic data encoding the quantum geometry. Eventually, the dynamics is implemented by summing over these data weighted by quantum amplitudes.

Beyond the theoretical elevator pitch, we face the challenge of turning spin foam models into a computational formalism: we need to be able to efficiently and reliably extract results from the theory, e.g. expectation values of observables describing a semi-classical geometry. Part of this question is to understand the impact of the discretisation and how to remove it in a suitable continuum limit [8–10]. Thus, we must perform explicit non-perturbative calculations on large triangulations with many degrees of freedom for which efficient numerical techniques are vital.

However, the before mentioned quantum, i.e. non-Wick-rotated, amplitudes pose a challenge: they are not positive (semi-)definite and can be complex, e.g. after introducing coherent states [11], and are typically highly oscillatory. Many methods in spin foams

developed and used so far are adapted to this. The derivations of asymptotic formulae of spin foam vertex amplitudes [12–17], which oscillate with the Regge action [18], exploit this oscillatory nature by employing stationary phase analysis. In recent years, this was generalized to larger triangulations using so-called complex critical points [19–22]. In this context complex refers to relevant configuration in addition to the dominating real critical points, where the former include curved configurations. Thus, this method suggest a route to avoid the so-called flatness problem [23–25].

However, asymptotic methods are valid approximations only for large representations, they are not accurate for small representations where geometry exhibits a more quantum behavior. The gap to the small representation regime is being bridged numerically in recent years [22, 26–28], with explicit calculations tackling triangulations with multiple simplices [29–31]. These works rely on an explicit numerical implementation of the representation theoretic calculations utilizing suitable analytical identities and efficient recoupling symbol libraries (mostly) avoiding truncations. The outstanding achievement is the creation of the library `sl2cfoam-next`¹ [32] with which amplitudes of the Lorentzian EPRL-FK model [33, 34] can be computed. These have been applied to a variety of physical systems [35–37]. Nevertheless, these calculations are costly, and what is more that these costs grow rapidly with the size of (boundary) representations as well as the size of triangulation, i.e. more degrees of freedom to explicitly sum over.

In an attempt to forego these costly computations and focus on the explicit path integral evaluation for larger triangulations, effective spin foams [38–42] were developed: instead of using the full amplitude, one assigns the exponentiated Regge action to each vertex restricting each vertex individually to a geometric 4-simplex. Such amplitudes are rapid to compute and the free resources can instead be used to explicitly sum over geometries. This sum is defined as a sum over all areas using the area Regge action [43–45]. To return to length Regge calculus second class simplicity constraints are modeled as Gaussian-shaped gluing constraints peaked on shape matching tetrahedra², such that two glued 4-simplices agree on the lengths assigned to the shared tetrahedron. This particular realization also suggests a reason (and how to avoid) the flatness problem [39]. One goal of this approach is then to investigate the emergence of semi-classical physics from the dynamics of the quantum theory, e.g. cosmology from Regge calculus [46–48]. One promising numerical method has been recently rediscovered [49], so-called acceleration operators [50, 51], that are efficient for computing sums of highly oscillating functions as they appear in spin foams. Related to effective spin foams are also so-called restricted spin foams [52–54], which restrict the spin foam path integral to particular configurations, e.g. cuboids, and utilizes the asymptotic formula to accelerate numerical calculations. This strategy was e.g. successful to investigate coarse graining flows [55–57], observables like the spectral dimension [58, 59] and matter coupling [60].

However, summing / integrating over a large numbers of variables explicitly becomes inefficient as the number of configurations in general grows exponentially. Monte Carlo

¹<https://github.com/qg-cpt-marseille/sl2cfoam-next>

²The Gaussians are peaked on matching 3d dihedral angles, more precisely two non-opposite ones. The four triangle areas agree by definition.

methods instead attempt to find an approximation by considering a finite number of samples of configurations, hence the costs do not scale with the number of variables. These samples are generated (semi-)randomly from a probability distribution, which for statistical systems is often derived from the partition function; this is then used to approximate expectation values. If this approximation is accurate for small sample sizes, the algorithm is often more efficient than explicit summation. Unfortunately, there is justified doubt that Monte Carlo methods are suitable for spin foams. The root of this doubt is that spin foams are quantum theories, i.e. they assign complex quantum amplitudes to each configuration. There is no obvious way how to analytically continue spin foams to purely statistical weights³. This is in contrast to causal dynamical triangulations [63] and causal set theory [64], where the theory can be continued to a purely statistical one, which can then be investigated by Markov chain Monte Carlo techniques. While this is a disadvantage for spin foams at the practical level, there are reasons not to Wick-rotate, since Euclidean quantum gravity models suffer from the conformal mode problem, where the Euclidean Einstein Hilbert action is not bounded from below⁴. Indeed, quantum amplitudes might be beneficial as they can lead to destructive interference, e.g. there are indications in causal set theory that quantum amplitudes suppress non-manifold-like causal sets [65].

However, if we aim to implement importance sampling Monte Carlo techniques in spin foams we face a technical and a fundamental problem. On the technical side we require a probability distribution, which is at best directly derived from the dynamics. Due to complex amplitudes, the spin foam partition function cannot be used directly to define such a distribution. Still, it is possible to “guess” a distribution, which can then be used to sample configurations. The simplest choice is the constant one, leading to random sampling, which is however not at all informed by the dynamics. It is the goal of this article to propose a new distribution for coherent intertwiners and apply this to the coherent spin foam vertex amplitude. Choosing a probability distribution however does not address the fundamental problem: the sign problem. If the functions we are investigating are alternating in sign / oscillating, contributions from different configurations will interfere destructively and cancel. However when sampling configurations we are likely to miss these cancellations. This might lead to slow convergence (if at all) and thus require a larger number of samples, which renders the algorithm less efficient. In our opinion, it is important to distinguish these two issues clearly: even for complex amplitudes we can define and apply Monte Carlo techniques by introducing a new probability distribution. This however does not address the sign problem, thus it does not guarantee that these methods efficiently produce reliable results.

Still, the sign problem does not rule out the usefulness of Monte Carlo methods for spin foams. Particular probability distributions, e.g. one derived from a Lefschetz thimble, do not suffer from the sign problem and can be used to investigate expectation values of observables [66]. A Lefschetz thimble is defined by deforming an integration contour such that the imaginary part of the integrand is constant on that contour, making the

³See [61, 62] for analytical continuations that relate Lorentzian and Euclidean signature models.

⁴Note that causal dynamical triangulations do not suffer from this by realizing that the space of (Wick-rotated) Lorentzian configurations is different from the set of Euclidean configurations.

expression non-oscillatory. Also, in particular situations, e.g. symmetry restrictions, the spin foam partition function can be positive semi-definite and be used for importance sampling [36, 52, 55, 56, 60]. Furthermore, a Monte Carlo algorithm can still provide acceptable results even if the sign problem is present. Indeed, there exist examples in the spin foam literature: in [31] a constant probability distribution, i.e. random sampling, is used to sample bulk representations and intertwiners. The results are convergent and the algorithm more efficient than simply summing over all possible values, which suggests that the sign problem may not be severe. We will confirm this impression in this article for the coherent $SU(2)$ vertex amplitude [26, 67], at least in most cases. However, note that the total number of variables sampled over is still fairly low; whether the sign problem remains tame for larger triangulations is not clear, but the indications is encouraging.

For completeness, a method that can be applied to systems suffering from the sign problem is tensor network renormalization [68–70]. Its approach to studying the dynamics is opposite to Monte Carlo: instead of considering the entire system through (probable) samples, one considers local amplitudes, the tensors, which are locally manipulated and coarse grained into effective amplitudes of composite degrees of freedom. Built into the coarse graining process is a truncation method to avoid exponentially growing numbers of degrees of freedom, where the truncations are done with respect to the relevance of the degrees of freedom derived from a singular value decomposition. Since the sums over degrees of freedom are performed without approximations, the sign problem does not manifest itself. However, challenges remain, e.g. algorithms for higher dimensional systems are intricate and are typically computationally costly. Moreover, one must work with tensors that have a finite index range; systems with continuous variables must be appropriately transformed, see [71] as an example of 2d lattice field theory. Quantum gravitational applications exist, e.g. in Lorentzian quantum Regge calculus [72], 2d analogue spin foam models [73–77] and 3d lattice gauge theories [78, 79]. The most recent work for 3d lattice gauge theories [80] utilizes the so-called fusion basis [81, 82], which is stable under coarse graining and well suited for studying expectation values of coarse (grained) observables.

The goal of this article is to propose an importance sampling algorithm for coherent intertwiners and use it to approximately compute spin foam amplitudes, here concretely the coherent $SU(2)$ BF theory vertex amplitude. To do so, we define a probability distribution from the absolute value of the coefficients of coherent intertwiners expressed in the orthonormal spin network basis. For coherent tetrahedra peaked on classical shapes, i.e. the coherent data satisfy the closure condition, these coefficients are sharply peaked and almost Gaussian. Sampling from such a distribution is straightforward. Since each intertwiner has its own independent distribution, generalizing this algorithm to the vertex amplitude (or larger triangulations with boundary) is immediate. We apply the algorithm the coherent BF vertex amplitude for different boundary data, e.g. the equilateral 4-simplex, and compare the results to the full calculation and the asymptotic formula. Overall, we find a good agreement of the results for a moderate number of samples. We see that the sign problem is present in determining the phase, but it is tame for most boundary data. Only when the amplitude is actually small, i.e. close to a root of the oscillations of the Regge action, we do observe convergence issues. In terms of computational times, the full calculation is

superior only at small representations, where actually only few configurations need to be summed over. Yet due to growing costs, the Monte Carlo method becomes efficient above spin $j \sim 10$ and provides a good approximation. The thus freed computational resources are invested into larger boundary spins.

This article is organized as follows: section 2 provides a brief introduction of spin foam models with a particular focus on the computation of the coherent vertex amplitude. Section 3 discusses the sign problem and describes the derivation of the probability distribution for coherent intertwiners and how intertwiner values are sampled. In section 4 we present the results for various boundary data, provide a brief comparison to random sampling and show measurements of computational time. Lastly, we summarize the results in section 5 and discuss how the algorithm can be generalized to larger 2-complexes, the Lorentzian EPRL model and bulk intertwiners.

2 Spin Foam numerics and coherent amplitudes

Since the main focus of this article is to introduce and discuss a new method to compute / approximate coherent spin foam vertex amplitudes, we will provide the necessary context to explain the calculation. For more detailed introductions and presentations of already existing numerical methods, we recommend several insightful reviews [10, 22].

As it is frequently the case, the definition of a path integral requires regularization; in spin foams this is done via the introduction of a discretization, a so-called 2-complex, which in most cases is chosen to be dual to a triangulation. Such a 2-complex is a collection of vertices v , edges e and faces f , to which we assign algebraic data. In 4d, a vertex is dual to a 4-simplex, an edge dual to a tetrahedron and a face dual to a triangle. Irreducible representations ρ_f are attached to the faces and describe their area, while intertwiners ι_e , invariant tensors in the tensor product of representations of faces sharing said edge, are assigned to the edges. The latter (partially) encode the shape of polyhedra, e.g. tetrahedra in a 4d triangulation [5]. One assignment of data to the 2-complex is a spin foam state, which prescribes the quantum geometry of this configuration. The path integral is implemented via the sum over all possible assignments of these data.

The dynamics are encoded in local amplitudes: we associate such amplitudes to vertices, edges and faces, where they only depend on the data assigned to this object. Generically, the spin foam partition function reads:

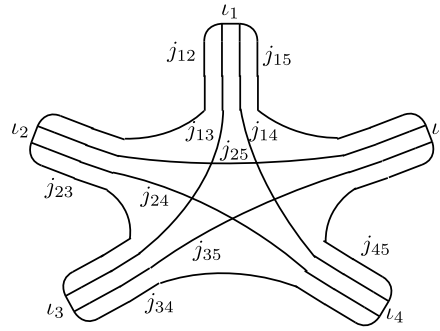
$$Z = \sum_{\rho_f} \sum_{\iota_e} \prod_f \mathcal{A}_f \prod_e \mathcal{A}_e \prod_v \mathcal{A}_v \quad , \quad (2.1)$$

where the sum is performed over all possible assignments of representations ρ_f and intertwiners ι_e . \mathcal{A}_f , \mathcal{A}_e and \mathcal{A}_v denote face, edge and vertex amplitudes respectively. While there are differences between the various spin foam models, similarities across the models exist, e.g. the face amplitude is usually given by the dimension of the representation and the edge amplitude is the inverse of the intertwiner norm. The most important amplitude is the vertex amplitude as it is associated with the (dual of) the fundamental building

blocks of quantum space-time, e.g. 4-simplices in 4d. It is at the center of attention of this article and we will discuss it in more detail now.

For concreteness, we will from now on specify our discussion to $SU(2)$ BF theory in 4d: while it is not a theory of quantum gravity its structure and coherent states are similar and relevant to the 4d (Lorentzian and Euclidean) EPRL model [33], such that the tools developed here for BF theory should be applicable and transferable to this more relevant model. The vertex amplitude is usually defined as follows: each edge in a spin foam encodes a projector onto the invariant subspace [1]. These projectors are written in terms of an orthonormal intertwiner basis, where one intertwiner is associated to each vertex of the edge. Each intertwiner has as many indices as the polyhedron has faces, so four in case of a tetrahedron. Then, we contract all intertwiners of a vertex with each other, i.e. we identify their indices when two intertwiners share a face and sum over them. This gives a number, the so-called vertex amplitude, which depends on spins and intertwiner basis elements. For a 4-simplex, we have five 4-valent intertwiners, where each intertwiner has one index contracted with any of the other four intertwiners. 4-valent $SU(2)$ intertwiners are not unique and can be labelled with one representation label using recoupling theory. The associated vertex amplitude is called the $SU(2)$ BF $\{15j\}$ -symbol; it depends on ten $SU(2)$ representations (called spins j_i) and five intertwiner labels.

Contracting intertwiners to compute the vertex amplitude is intuitive as it matches how we would combinatorially 4-simplex from tetrahedra. However, this explicit contraction is computationally costly, as we have to sum over ten magnetic indices. Moreover, this range of indices grows with the size of the spins, too, increasing the costs further. Instead, the $\{15j\}$ -symbol can be concisely expressed in terms of $SU(2)$ $\{6j\}$ -symbols [29]:



$$= (-1)^{\sum_i j_i + \sum_i l_i} \sum_x (2x+1) \times$$

$$\times \begin{Bmatrix} l_1 & j_{25} & x \\ l_5 & j_{14} & j_{15} \end{Bmatrix} \begin{Bmatrix} j_{14} & l_5 & x \\ j_{35} & l_4 & j_{45} \end{Bmatrix} \begin{Bmatrix} l_4 & j_{35} & x \\ l_3 & j_{24} & j_{34} \end{Bmatrix} \begin{Bmatrix} j_{24} & l_3 & x \\ j_{13} & l_2 & j_{23} \end{Bmatrix} \begin{Bmatrix} l_2 & j_{13} & x \\ l_1 & j_{25} & j_{12} \end{Bmatrix} . \quad (2.2)$$

This expression is highly efficient for numerical implementations: highly optimized libraries for computing the $\{6j\}$ -symbol exist, e.g. `WignerSymbols`⁵ in `Julia`, and the sum over one auxiliary label x is bounded by the spins.

So far, we only concerned ourselves with a single $\{15j\}$ -symbol. When studying the large spin behavior of spin foams, which is often referred to as the semi-classical limit (at least for a single 4-simplex), we are rather interested in states peaked on Regge geome-

⁵<https://github.com/Jutho/WignerSymbols.jl> .

tries, i.e. classical simplices, as these play a dominant role in this limit [67]. Such Regge geometries are encoded via coherent intertwiners [11], a group averaged tensor product of $SU(2)$ Perelomov coherent states [83]. These coherent states form an overcomplete basis and the group integration can be written as a sum over orthonormal intertwiners. This generalizes straightforwardly to the coherent vertex amplitude, which can be written as a superposition of $\{15j\}$ -symbols. We briefly review this in the next section.

2.1 Coherent $SU(2)$ vertex amplitude

$SU(2)$ coherent states play a crucial role in the asymptotic analysis. They are defined as maximum or minimum weight states, where the states $|j, j\rangle$ or $|j, -j\rangle$ respectively are used as reference states. As these states are eigenstates of J_z for maximum / minimum weight, they are associated with the direction \vec{e}_z . We will use the maximum weight eigenstate through the entirety of this paper.

We can peak this state on a different direction by acting on it with a group element, via the associated Wigner matrix.

$$|j, \vec{n}\rangle = D^j(g_{\vec{n}})|j, j\rangle = \text{---} \bullet \quad j, \vec{n} \quad . \quad (2.3)$$

$g_{\vec{n}}$ is a group element in $SU(2)/U(1)$, which encodes the rotation from \vec{e}_z (the reference state) to \vec{n} ; the coherent states are only defined up to a phase. Combining several of these coherent states with a group integration defines a coherent Livine-Speziale intertwiner [11]. For concreteness, we consider a 4-valent one to describe tetrahedra:

$$\iota(\{j_i\}, \{\vec{n}_i\}) = \int_{SU(2)} dg \bigotimes_{i=1}^4 D^{j_i}(g) |j_i, \vec{n}_i\rangle = \{j_i\}, \{\vec{n}_i\} \quad \text{---} \boxed{\quad} \text{---} \quad , \quad (2.4)$$

where we represent the group integration by a box over all strands.

The coherent vertex amplitude is typically defined as the contraction of five such intertwiners:

$$\begin{aligned} \text{Diagram} &= \int_{SU(2)} \prod_a dg_a \prod_{a < b} \langle j_{ab}, -\vec{n}_{ba} | D^{j_{ab}}(g_b^{-1}) D^{j_{ab}}(g_a) | j_{ab}, \vec{n}_{ab} \rangle \quad (2.5) \\ &= \int_{SU(2)} \prod_a dg_a \prod_{a < b} \left(\langle \tfrac{1}{2}, -\vec{n}_{ba} | g_b^{-1} g_a | \tfrac{1}{2}, \vec{n}_{ab} \rangle \right)^{2j_{ab}} , \end{aligned}$$

where we have used the fact that the coherent states are maximum weight states in the second line. This explicit representation in terms of group integrations is ideally suited for applying a stationary phase approximation as the inner products are highly oscillatory, from which spin foam asymptotics were derived in a plethora of contexts [13–17, 67]. On the other hand, the oscillatory nature is challenging for explicit numerical calculations.

One attempt would be to perform four $SU(2)$ integrations (one can be dropped due to gauge invariance) numerically, using e.g. the Cuba package [84], which would be a

labels, i.e. $(2j + 1)^5$ possibilities. To compute each $\{15j\}$ -symbol we have to sum over an auxiliary label with range proportional to j . Thus, overall computing and saving the array of all variants of the $\{15j\}$ -symbol scales proportional to j^6 . The following contractions of this array with five vectors of coherent intertwiner components is subleading in comparison: the first contraction scales with $(2j + 1)^5$ since we are summing over one label while keeping four ones fixed. The following contractions scale more favourably. In summary, the full calculation scales exponentially when homogeneously scaling up all spins for general boundary data. To illustrate the scope, for all spins $j = 50$, the array storing the $\{15j\}$ -symbols for all intertwiner labels contains $\sim 3 \cdot 10^8$ entries, which requires a significant computational time to compute and a large amount of memory to store⁶. This poses a challenge to computing the amplitude for larger 2-complexes.

Hence the question arises, whether we can optimize these calculations further or find suitable approximations. In this article we pursue the question whether we can truncate the sum over intertwiners, therefore reducing the numerical costs. Indeed, for sufficiently large spins and coherent states peaked on geometric tetrahedra, the absolute value of the coherent intertwiner coefficients c_l are typically sharply peaked, such that labels far away from the peak should be safe to ignore. This idea was first formulated in [27], where labels were truncated if they are less relevant than a chosen cut-off relative to the peak. Choosing this cut-off then controls the quality of the approximation versus the costs of the calculation. Yet, explicit testing of different cut-offs is necessary to see whether the approximation can be trusted.

In this article, we build upon this idea and use the absolute value of c_l to define a probability distribution for the intertwiner labels for a Markov Chain Monte Carlo algorithm. From this distribution, we sample intertwiner labels according to their relevance inferred from the coherent states and approximate the coherent vertex amplitude without introducing a cut-off by hand. The approximation should then improve by increasing the number of samples and eventually converge to the actual result. If the algorithm is converging quickly, it should provide a good approximation utilizing a fraction of configurations compared to the full calculation. Therefore, a convergent Monte Carlo algorithm promises to free computational resources, which can instead be used to investigate spin foams defined on larger 2-complexes. However, the main obstacle for convergence is the so-called sign problem. In the next section, we briefly review Monte Carlo methods and the sign problem, explain why it is present in spin foams and briefly discuss the sampling procedure for coherent intertwiner labels.

3 Monte Carlo and the sign problem

In physics Monte Carlo methods are an efficient and useful tool to study statistical systems with a large number of degrees of freedom. These systems are described by high dimensional integrals or sums over all possible configurations of its variables, which typically

⁶Writing the contraction as for loops reduces the memory costs, but is typically far slower. Tensor network contractions make use of highly optimized linear algebra operations. Further speed up can be achieved by utilizing GPUs [32].

cannot be evaluated analytically or calculated numerically by brute force. Instead, Markov chain Monte Carlo methods sample typical configurations from the probability distribution defining the statistical theory. With sufficiently many such samples one may well approximate expectation values of observables of the system and extract physical information. The key advantage is that this algorithm scales with the number of samples rather than exponentially with the number of variables.

These samples are generated in a random process, take e.g. the Metropolis-Hastings algorithm [86, 87]. Starting from a random configuration, a new configuration is proposed by randomly deviating from the previous one by a given set of moves. Then the probabilities of these two configurations are compared; if the new configuration is more probable it is always accepted. If it is not, then it is accepted only with a certain probability. This method must be implemented with care to obtain correct and reliable results, e.g. one must implement detailed balance to ensure that one is indeed sampling with respect to the probability distribution of the system. Moreover, the proposal of new configurations must be ergodic, i.e. it must be possible to reach any configuration of the system (given enough time). Finally, one must ensure that the algorithm explores a sufficiently large part of the configuration space. This is often gauged by the acceptance rate of new configurations.

3.1 Complex amplitudes and the sign problem

Not all physical theories are statistical theories. While many theories, e.g. lattice field theories (at zero temperature and without fermions) and causal dynamical triangulations [63], can be analytically continued from a quantum to a statistical theory, this is not the case for many quantum theories including spin foam models (unless some particular symmetry restrictions are considered [88]). The consequences are two-fold: first, the partition function does not define a probability distribution and thus cannot be used to sample configurations. The second and more severe consequence is the so-called sign problem: alternating / oscillating amplitudes can lead to contributions cancelling each other. If the sign problem is severe, we must take a lot of samples to capture this effect and hopefully obtain a convergent result. Of course, more samples come with larger numerical costs, such that the algorithm is less efficient.

It is important to distinguish these two aspects: for complex amplitudes we have no probability distribution readily available and the sign problem is present. Still, Monte Carlo methods might be useful for exploring the dynamics of the model if the sign problem is tame. To do so, one must propose a new probability distribution. A simple possibility is the constant distribution, which assigns the same weight to all configurations, but usually it is beneficial to use a distribution fitting the dynamics of the system, which again can be challenging for oscillating functions. Note however, that defining a new distribution does not solve the sign problem.

To illustrate this consider the so-called reweighting procedure [89, 90]. Consider a physical system with complex amplitude \mathcal{A} for variables ϕ_i . For concreteness, we consider the ϕ_i to have a discrete spectrum; then the partition function and expectation values of

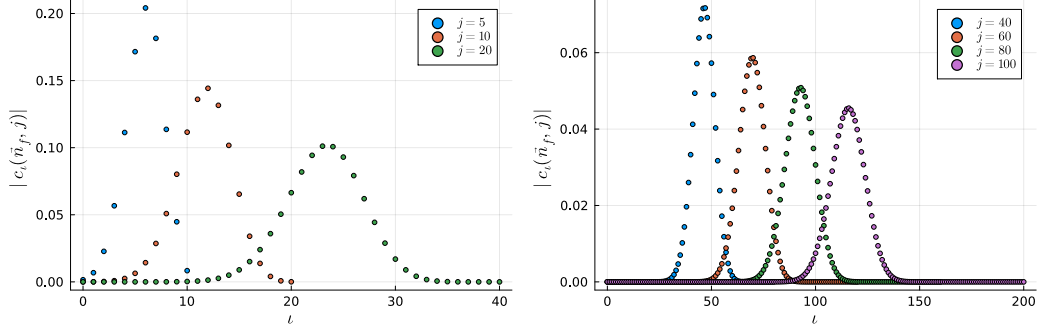


Figure 1: Coherent intertwiner coefficients for equilateral tetrahedra. *Left:* spins $j = 5, 10, 20$. *Right:* spins $j = 40, 60, 80, 100$

observables are (formally) defined by

$$Z = \sum_{\{\phi_i\}} \mathcal{A}(\{\phi_i\}) \quad , \quad \langle \mathcal{O} \rangle_{\mathcal{A}} = \frac{1}{Z} \sum_{\{\phi_i\}} \mathcal{O}(\{\phi_i\}) \mathcal{A}(\{\phi_i\}) \quad . \quad (3.1)$$

From \mathcal{A} , we can define a probability distribution by taking its absolute value with normalization $\frac{1}{Z}$. With this probability distribution, we compute $\langle \mathcal{O} \rangle_{\mathcal{A}}$ as follows:

$$\langle \mathcal{O} \rangle_{\mathcal{A}} = \frac{1}{Z} \frac{Z'}{Z'} \sum_{\{\phi_i\}} \mathcal{O}(\{\phi_i\}) e^{i\varphi_{\mathcal{A}}} |\mathcal{A}(\{\phi_i\})| = \frac{\langle e^{i\varphi_{\mathcal{A}}} \mathcal{O} \rangle_{|\mathcal{A}|}}{\langle e^{i\varphi_{\mathcal{A}}} \rangle_{|\mathcal{A}|}} \quad , \quad (3.2)$$

where $\varphi_{\mathcal{A}}$ denotes the phase of \mathcal{A} (for a specific configuration $\{\phi_i\}$), and we denote by $\langle \mathcal{O} \rangle_{|\mathcal{A}|}$ the expectation value of \mathcal{O} computed in the distribution defined by $|\mathcal{A}|$. Essentially, we absorb the phase $\varphi_{\mathcal{A}}$ into the observable and compute it in the distribution given by $|\mathcal{A}|$. Since this is not the original expression, we must correct this by dividing by the expectation value of the phase. Both expectation values are now in principle computable using importance sampling Monte Carlo techniques, but the sign problem enters here: if the sign problem is severe, the expectation value of the phase is small or zero. Then, the expectation value computed in this way will not converge and the result cannot be trusted.

Eventually, we do not know how severe the sign problem in spin foams is. In the following we propose a probability distribution for coherent (boundary) intertwiners, with which we approximate the coherent vertex amplitude. The results suggest that the sign problem for this amplitude is not severe (in most cases).

3.2 Probability distribution from coherent intertwiners

In eq. Eq. (2.8), the coherent vertex amplitude is written as the contraction of the $\{15j\}$ -symbol with the components of coherent intertwiners c_l , see eq. Eq. (2.7). The goal is to approximate the sum over intertwiners using Monte Carlo methods by a number of samples, which hopefully converges for significantly fewer samples than the total number of configurations. Towards defining a probability distribution suitable for this amplitude, we consider the coherent intertwiner expanded in orthonormal intertwiners more closely.

The intertwiner components are in general complex, as can be expected from an over-complete basis. Their absolute value on the other hand, see fig. 1, has a pronounced peak, which becomes sharper (relative to the total range of intertwiner labels) as the spins are uniformly increased. Thus, for large spins, this is an excellent choice to define a probability distribution, yet it also reveals a weakness. For small spins, the peak is so broad that it covers the entire range of all intertwiner labels. Hence, all intertwiners labels are similarly relevant (roughly same order of magnitude) and the potential to save computational time by sampling is low. Fortunately, the range of intertwiner labels is then still low such that explicit summation is viable. Therefore, we should rather consider the Monte Carlo methods to complement the full calculations at large spins. The final step to obtain the probability distribution is to fix the normalization, which is simply given by the inverse of the sum of all $|c_\ell|$. In the next section we briefly discuss the sampling procedure.

3.2.1 Sampling coherent intertwiners

The almost Gaussian distribution of the probability measure is ideal for sampling. Thus, we keep this discussion brief. When proposing a new configuration, we essentially shift the intertwiner label by a random integer. The simplest variant is to shift it by ± 1 , but larger (random) shifts are possible. Either variant leads to an ergodic algorithm, yet they will differ in the acceptance rate of new proposals. If the range of possible shifts is larger, there will be more proposals that shift the intertwiner labels to a value far away from the peak. These are improbable, therefore they will be rejected in most cases. In particular in systems with a large number of degrees of freedom, the acceptance rate is a good gauge to see whether one is exploring a sufficiently large part of the configuration space and choose the proposal of new configurations appropriately. This is important, as one does not want to get stuck in a local maximum. Here we are sampling a one-dimensional system with a simple distribution, where this issue appears to be less relevant.

For the almost Gaussian probability distribution proposed here, these considerations appear to be far less relevant. In fig. 2 we plot histograms of sampled intertwiner labels for the distribution given by an equilateral tetrahedron for all spins $j = 50$. The two sampling methods differ in the proposed shift size, for one it is ± 1 , for the other it is a random number between 1 and $\frac{1}{3}$ of the total intertwiner range. Qualitatively the histograms look similar and are able to sample labels of the whole peak and the beginning of the tails. A larger step size, with a lower acceptance rate, should be more suitable at sampling the tails of the distribution. However, due to the low probability of these values, we expect this to become noticeable only for a larger number of samples.

For small spins, the proposal scheme for a larger step size requires more scrutiny. Then, the peak of the coherent intertwiner essentially covers the whole intertwiner range and each intertwiner value has a relevant probability. As a result, the potential to save on computational time by using Monte Carlo methods is reduced. If we now choose a maximal step size that is e.g. half or a third of the total intertwiner range, we will propose values outside the permitted range. This could be remedied by simply setting the value by hand to the value at the boundary. However, this choice leads to an overemphasis of those boundary values, which is shown in the histogram in fig. 3. This is due to the fact that the

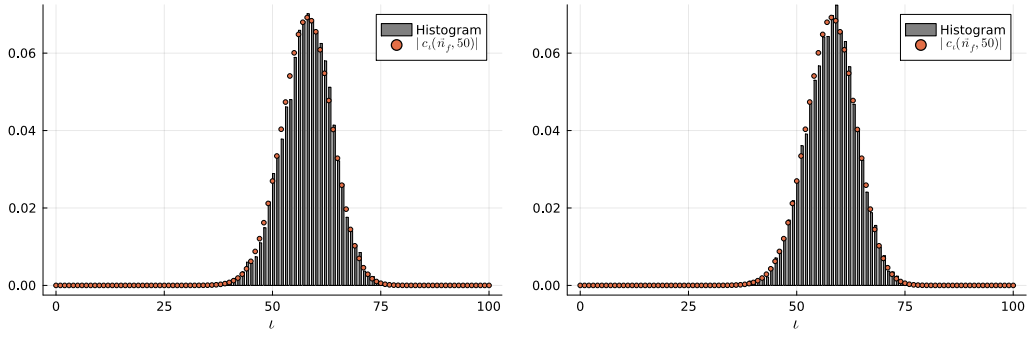


Figure 2: Normalized histogram sampling equilateral tetrahedra for $j = 50$. 10^4 thermalization steps, 500 steps between taking samples. *Left:* Step size 1 when proposing new configuration. *Right:* Maximal step size ~ 50 when proposing new configuration.

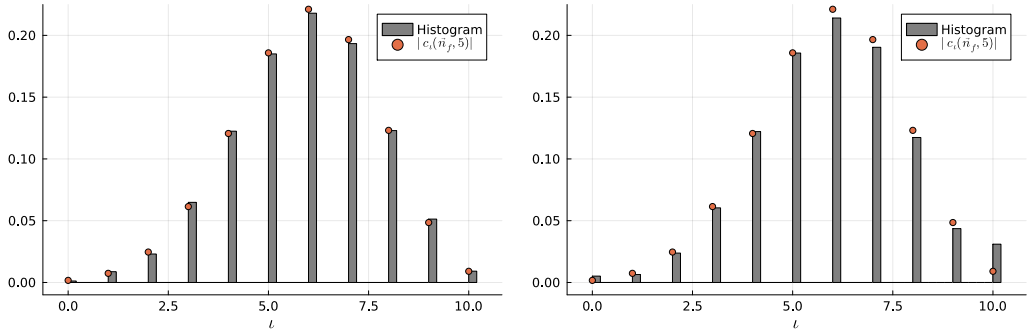


Figure 3: Normalized histogram sampling equilateral tetrahedra for $j = 5$. 10^4 thermalization steps, 500 steps between taking samples. *Left:* Step size 1 when proposing new configuration. *Right:* Maximal step size ~ 50 when proposing new configuration. The overemphasis of values on the boundary is visible.

proposal method violates detailed balance, as it proposes the boundary values more than other values⁷. We can avoid this by using a step size of ± 1 .

The important take away message is that the algorithm is capable of sampling values of the coherent state peak including the tails, where the sampling is only determined by the probability of the intertwiner labels; no cut-off is introduced by hand. Therefore, this is a different implementation of the idea introduced in [27] to approximate the coherent states by truncating the intertwiner degrees of freedom. However, it is also clear that this sampling algorithm becomes efficient compared to the full calculation at large spins when the coherent states are strongly peaked.

Beyond these details, the sampling in the Metropolis-Hastings algorithm is fairly standard. First, we make sure the system has thermalized, for which we typically use 10^4 steps. Between samples we usually include around $2 \cdot 10^3$ steps to reduce cross correlations between samples.

⁷We can fix this flaw by using “periodic boundary conditions” on the intertwiner values. Instead of ending at the minimal / maximal intertwiner range, we continue at the other end of the distribution.

In the next section we discuss how to apply this sampling algorithm to the coherent $SU(2)$ vertex amplitude and present results for different sets of boundary data. We compare these results to the full calculation, the asymptotic formula and results found by random sampling.

4 Approximating coherent vertex amplitudes

So far, we have discussed how to define a probability distribution for a single coherent tetrahedron and how to sample from it. The coherent vertex amplitude is defined as the contraction of five such tetrahedra against the $SU(2)$ $\{15j\}$ -symbol. We will approximate the coherent amplitude by sampling each intertwiner label individually. Similarly, we can straightforwardly generalize this method to arbitrarily large 2-complexes with boundary for coherent state boundary data.

The key point we must address is that the probability distribution we intend to use is not part of the coherent vertex amplitude. To explain how we overcome this, consider a simple example, a 1d integral $\int_0^1 dx f(x)$ over the finite interval $[0, 1]$. We can approximate the integral by sampling a probability distribution P with $\int_0^1 dx P(x) = 1$ as follows:

$$\int_0^1 dx f(x) = \int_0^1 \frac{f(x)}{P(x)} P(x) \approx \frac{1}{N} \sum_{i=1}^N \frac{f(x_i)}{P(x_i)} . \quad (4.1)$$

In the final step, we approximate the expression by summing over N samples $\{x_i\}$ generated from P . Note that sampling from P modifies the original expression: we sample points x_i more frequently which are more probable according to P , while we sample points less frequently which are less probable. Since this is not present in the original expression, we compensate for this by evaluating $\frac{f}{P}$ for these samples, i.e. samples which are less probable in P contribute more to the approximation. So far we have not specified the distribution P and a priori it is not clear whether P is suitable for efficiently approximating the desired expression. The ideal P would be such that the fraction $\frac{f}{P}$ is constant $\forall x \in [0, 1]$, resulting in an exact result for any number of samples. Yet this would imply that we have already solved the integral defeating the purpose of studying it with Monte Carlo methods in the first place. Numerical integration algorithms attempt to find such optimal distributions [84]. For rapidly oscillating functions, for which Monte Carlo methods suffer from the sign problem, probability distributions adapted to the functions are challenging to define and yet it is not clear whether this leads to a good convergence. Instead one can guess a simpler to define distribution, but convergence remains an open question. A concrete example for a simple distribution is the constant one, which leads to random sampling.

Random sampling of intertwiners One of the simplest probability distributions we can propose is the constant probability for all intertwiner labels. For discrete variables such as the orthonormal intertwiner labels, the probability distribution is simply given by the inverse of the number of possible intertwiner labels. For a single intertwiner label, this

reads:

$$\sum_{\iota} f(\iota) = \sum_{\iota} \frac{f(\iota)}{P(\iota)} P(\iota) = \sum_{\iota} n^{\iota} f(\iota) \frac{1}{n^{\iota}} \approx \frac{n^{\iota}}{N} \sum_{i=1}^N f(i) \quad , \quad (4.2)$$

where n^{ι} denotes the total number of possible intertwiner labels. N is the number of samples; the larger N , the better the approximation will become, however convergence might be slow. From such a constant distribution, we can simply generate samples by randomly selecting one among all the possibilities, hence the name random sampling.

At first sight, random sampling appears paradoxical; it is geared towards approximating the sum / integral of a constant function, for which Monte Carlo methods are not necessary in the first place. From a practical point of view, a few advantages emerge common for Monte Carlo methods. It is straightforward to implement in most situations⁸ and the numerical costs scale with the number of samples rather than the number of variables in the system. In particular for systems with many variables, random sampling can provide a reasonable approximation at less costs than brute force summation. However, it is a priori not clear how many samples will be necessary for a convergent result. The expectation is that less samples are necessary to obtain a convergent result if one instead uses importance sampling of a distribution adapted to the problem at hand. In the next paragraph, we expand on the numerical challenge of computing the coherent vertex amplitude and how we choose a probability distribution to more efficiently approximate it.

Importance sampling coherent intertwiners As we describe in detail in section 3, our aim is to sample intertwiner degrees of freedom with respect to the absolute value of coherent intertwiners $|c_{\iota}(j_i, \vec{n}_i)|$, precisely the coefficient of coherent intertwiners expressed in the orthonormal intertwiner basis. In general, we could choose any coherent state to define such a probability distribution⁹, but this would not be adapted to the calculation at hand. Instead we pick the states encoded in the boundary data and rewrite the vertex

⁸Determining the total number of possibilities can be intricate, e.g. when implementing coupling rules of representations in spin foams, see also [31]. Alternatively, we can simply allow all possible values of variables and set forbidden configurations to give vanishing contributions. Yet, this leads to slower convergence.

⁹Using coherent states which describe tetrahedra with non-closing normals are likely not suitable, as their intertwiner norm is exponentially suppressed as one uniformly scales up its spins.

amplitude as follows:

$$\begin{aligned}
& \text{Diagram 1} = \sum_{\{\iota_i\}} \prod_{k=1}^5 c_{\iota_k}(j_i, \vec{n}_k) \quad \text{Diagram 2} \tag{4.3} \\
& = \sum_{\{\iota_i\}} \prod_{k=1}^5 \frac{n_k}{|c_{\iota_k}(j_i, \vec{n}_k)|} \frac{|c_{\iota_k}(j_i, \vec{n}_k)|}{n_k} \prod_{k=1}^5 c_{\iota_k}(j_i, \vec{n}_k) \quad \text{Diagram 3} \\
& \approx \frac{1}{N} \sum_{x=1}^N \prod_{k=1}^5 n_k \frac{c_{\iota_k(x)}(j_i, \vec{n}_k)}{|c_{\iota_k(x)}(j_i, \vec{n}_k)|} \quad \text{Diagram 4} .
\end{aligned}$$

In the second line, we insert the probability distribution and its inverse. Then, in the third line, we approximate the full expression by sampling with respect to the distribution with N samples in total. The final expression we evaluate for the samples of intertwiners depends then on the phase of the coefficients c_{ι} and the overall normalisations.

Before presenting results of this sampling method, let us briefly revisit the properties of the coherent vertex amplitude and its sign problem, which is not solved by this sampling method.

4.1 Sign problem in the coherent vertex amplitude

While the $\text{SU}(2)$ $\{15j\}$ -symbol is defined to be real, the coherent vertex amplitude is generically complex. This is due to the introduction of the complex overcomplete basis of Perelomov coherent states, which are however essential to define coherent tetrahedra states that are peaked on the shape of classical polyhedra. Unfortunately, it is also the reason that we cannot simply use spin foam amplitudes itself to define a probability distribution¹⁰. On the other hand, coherent $\text{SU}(2)$ states are only defined up to a phase. Similarly the coherent vertex amplitude is defined up to a global phase [26], and we choose it such that the coherent amplitude is purely real. In the numerical setting, this can be done as follows: we compute the full amplitude for a spin configuration and choice of coherent states and compute its phase. Under uniform scaling of spins (keeping the \vec{n}_i fixed), this phase changes linearly, such that we use it to turn amplitude real for all spins. Thus, we

¹⁰Technically this already applies to the $\{15j\}$ -symbol, as it can be negative.

numerically obtain a real amplitude for all spins with a tiny imaginary part limited by numerical precision. Moreover, for Regge-geometry boundary data, the real part oscillates with the Regge action [18] of the described 4-simplex (under uniform scaling of boundary areas).

The goal of our Monte Carlo algorithm is to approximate the full amplitude, i.e. reproduce the significant real part and a vanishing imaginary part. As we will see below, this reveals the strengths and weaknesses of our algorithm. While the real part (for almost all cases) shows a good convergence and accuracy compared to the full calculation and the asymptotic approximation (for large spins), reproducing the oscillating behavior for Regge-geometric boundary data, the imaginary part is more subtle. While it is in most cases significantly smaller than the real part, typically up to three orders of magnitude, it is not as small as in the full calculation. This suggests that the convergence of the imaginary part is slower than the real part and more samples are necessary to approximate it better. We expect this behavior: the individual summands of the coherent vertex amplitude are generically complex. While the real parts sum up to a non-vanishing number, their imaginary parts exactly cancel due to the choice of global phase. This is the literal definition of the sign problem, and Monte Carlo methods suffer from slow convergence due to sampling of configurations. Still, for the coherent vertex amplitude the convergence of the imaginary part is acceptable. If we would only consider the absolute value of the amplitude, this convergence issue would remain unnoticed.

However, we will also see that for some boundary data that the real part suffers from the sing problem. These are precisely the boundary spins where the entire amplitude almost vanishes, i.e. close to the roots of the cosine of the Regge action. The same argument as for the imaginary part holds here as well, as (most of) the summands in the vertex amplitude cancel each other.

In the following we will introduce the boundary data to a few geometric Euclidean 4-simplices, e.g. the equilateral 4-simplex and an isosceles 4-simplex, and compute the amplitude using importance sampling Monte Carlo. Since Monte Carlo methods are inherently random, we need to provide an error estimate. To do so, we take 10^5 samples and repeat this process 30 times. We compute the mean and variance of these estimates, thus using $3 \cdot 10^6$ samples in total for each set of boundary data. Additionally, for the equilateral 4-simplex, we will also show results for random sampling to give an impression of convergence. Moreover, we will compare these results to the full calculation where it is computationally feasible and the asymptotic amplitude to leading order.

4.2 Results

The main results are shown in plots of the rescaled vertex amplitude, where we account for the asymptotic scaling behavior of the vertex amplitude (λ^{-6} for all $j \rightarrow \lambda j$). These plots nicely show the oscillatory nature of the vertex amplitude, and, at a glance, we get a good impression of the accuracy of the Monte Carlo results in most cases including an error estimate. However, from these plots, it is difficult to see deviations if the real part of the amplitude is small, and how small the imaginary part of the amplitude is. Therefore, we add a logarithmic plot of the absolute value. Finally, we also add a plot of the relative

error ϵ defined as:

$$\epsilon = \left| \frac{\mathcal{A}_v^{\text{MC}} - \mathcal{A}_v}{\mathcal{A}_v} \right| . \quad (4.4)$$

The relative error is computed for the full amplitude as well as its asymptotic approximation.

For all the plots, we use the same colors. The full calculation is in orange, its asymptotic approximation in yellow; the same colors apply to the relative errors. Monte Carlo results are shown as crosses with error bars (exception the logarithmic plots), where blue crosses show the real part and purple crosses the imaginary part.

4.2.1 Equilateral 4-simplex

The equilateral 4-simplex is one of the simplest examples of the coherent vertex amplitude. In Regge calculus it is prescribed by having the same edge lengths for all its ten edges. All of its 4d dihedral angles are equal and also all of its sub-simplices are equilateral as well. In spin foams, it is described by choosing all ten spins, related to its areas, to be the same. We prescribe the normal vectors for the triangles in each tetrahedron as follows:

$$\begin{aligned} \vec{n}_{12} &= (0, 0, 1) , & \vec{n}_{13} &= \left(0, 0.94280, -\frac{1}{3} \right) , \\ \vec{n}_{14} &= \left(0.816497, -0.47140, -\frac{1}{3} \right) , & \vec{n}_{15} &= \left(-0.816497, -0.47140, -\frac{1}{3} \right) . \end{aligned} \quad (4.5)$$

Here we choose the same normal vectors for each tetrahedron. Instead one could also use the twisted spike configuration [26], where the normal vectors are chosen to be pairwise anti-parallel, i.e. $\vec{n}_{ab} = -\vec{n}_{ba}$. Both choices differ by a global phase, which we are free to choose.

Before presenting the results of our importance sampling algorithm, we briefly show results for random sampling to provide a comparison of accuracy and convergence of the results

Random sampling For random sampling we present the results of two runs: both have 30 repetitions in total with 10^5 and 10^6 samples each respectively. From the results of these runs we compute the mean and the variance of the amplitude to estimate an error; the mean is thus computed from $3 \cdot 10^6$ and $3 \cdot 10^7$ samples in total respectively. In fig. 4 we plot the rescaled results from both runs and compare to the full numerical calculation and the semi-classical amplitude. Since the plots are busy in particular due to error bars, we split them into two intervals: from $j = 0$ to $j = 30$ to compare to the full amplitude and from $j = 30.5$ to $j = 50$ to compare to the asymptotic formula. For the simulations with 10^5 samples per run, the real part agrees well with the full calculation up to spins $j \sim 15$, yet for larger spins deviations are visible and the variance is large. The same holds in comparison to the asymptotic formula. As expected, convergence for the imaginary part is worse and for spins $j > 20$ the imaginary part is frequently of the same order of magnitude as the real part. Thus, more samples are clearly necessary. Indeed, the runs with 10^6 samples significantly improve the results and the agreement with full and semi-classical formula is

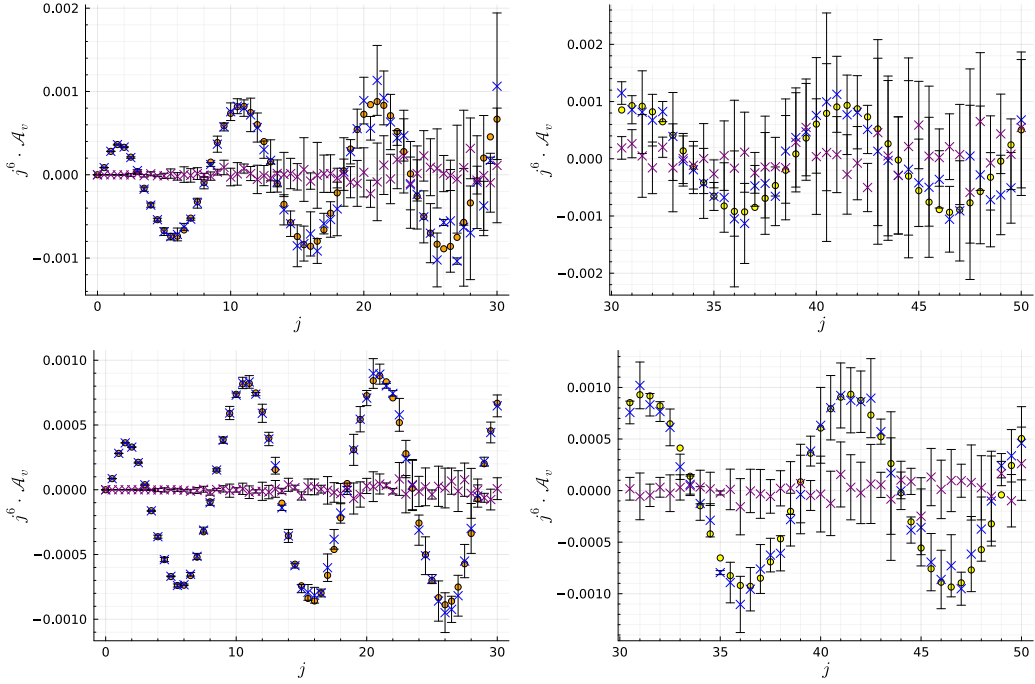


Figure 4: Random sampling results for equilateral coherent vertex amplitude for 30 runs, top plots show 10^5 samples per run, bottom plots 10^6 samples per run. j labels the spins. *Left:* comparison for spins up to $j = 30$ with full numerical calculation. *Right:* Comparison from $j = 30.5$ up to $j = 50$ to asymptotic formula.

decent. However, the variance of the real part becomes large for $j > 40$. The imaginary part is improved as well, but shows non-vanishing values already early on. Nevertheless, while we observe inaccuracies, in most cases random sampling reproduces the correct order of magnitude (recall that the results are rescaled by j^6), and for $j > 20$ the results are obtained at lower computational costs than the full calculation.

These results are also confirmed in the logarithmic plots and relative error, see fig. 5. The logarithmic plots nicely show that random sampling adequately reproduces the real part, unless it almost vanishes compared to boundary spins of similar size; this indicates that the sign problem is more severe for these cases. The agreement gets worse as we increase the spins j , which must be compensated by increasing the number of samples. Convergence of the imaginary part is worse; in particular for large spins it is often of the same order of magnitude as the real part. We also see that the relative error for the real part grows for larger spins. For small spins, it is fairly low, but quickly increases for growing spins. Still in many cases it is at or below 10%, which could be improved by more samples. To improve on both the real and imaginary part, we must increase the number of samples further, in particular for large spins.

To summarize, we can draw two conclusions for random sampling. First, it is able to decently approximate the coherent vertex amplitude even for relatively small number of samples. While the variance is high and increases with larger spins, the relative error remains under control. This is already a achievement since these results are obtained at

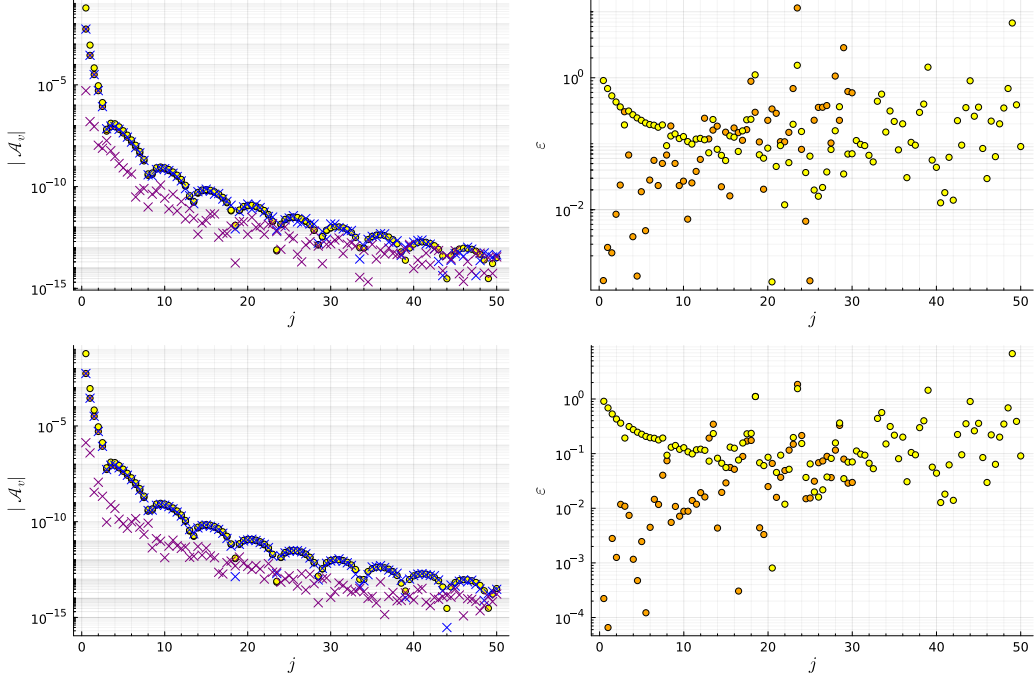


Figure 5: Random sampling of equilateral vertex amplitude, top shows results from 30 runs with 10^5 samples, top results for 30 runs with 10^6 samples. *Left:* Logarithmic plot of absolute value of vertex amplitude \mathcal{A}_v . *Right:* Relative error ϵ of real part of \mathcal{A}_v .

significantly lower costs compared to the full calculation. The second insight is that the sign problem does not appear to be too severe, at least for the real part of the amplitude.

In the following, we will improve on these results with our importance sampling algorithm using the boundary coherent states, in particular in terms of accuracy for the same number of samples. Furthermore, we also increase the boundary spins further.

Results of multiple runs and error estimate Similar to random sampling, we present the data for 30 runs, each with 10^5 samples; hence $3 \cdot 10^6$ samples in total. The results range from $j = 0$ to $j = 250$ and are presented in fig. 6. We have split the plots around $j = 35$ between the results for the full and the asymptotic amplitude. Let us discuss the top plots first, which show the rescaled amplitude. Let us start with real part.

Overall, the Monte Carlo results are barely distinguishable from the full calculation, and also when compared to the asymptotic formula the results agree well besides a few deviations. In particular for spin around $j \sim 40$ we see a few deviations, probably because the asymptotic formula is not yet accurate enough. The excellent agreement can also be seen in the logarithmic plots, with a few exceptions. These are again the cases for which the amplitude itself almost vanishes and where the sign problem is more severe. Another remarkable feature are the relatively small variances, in particular for small spins. For larger spins, we irregularly see slightly larger variances; this is a first indication that more samples / more runs might be necessary to improve the results.

The behavior of the imaginary part is more intricate. In the rescaled plots it appears

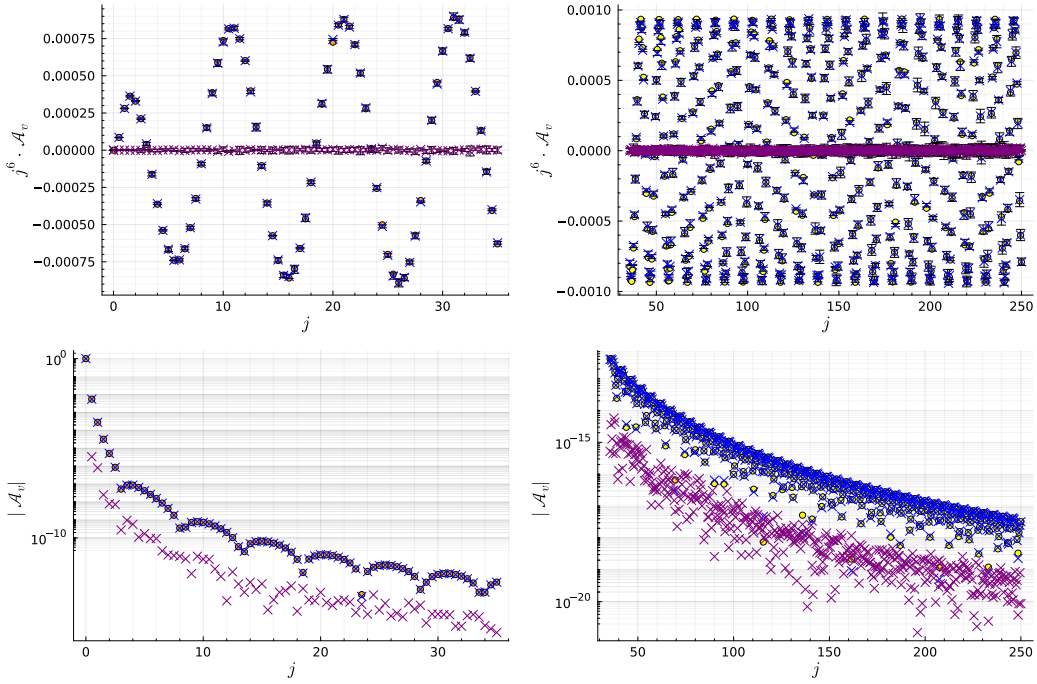


Figure 6: Equilateral vertex amplitude approximated via coherent state importance sampling. Top plots show the rescaled amplitude, bottom plots show logarithmic plots of absolute value. *Left:* Spins j from 0 to 35. *Right:* Spins j from 35.5 to 250.

to be small, typically much smaller than the real part with rather small variances. This continues for large spins, yet we observe that it deviates further from zero and also that the variances grow, while typically being much smaller than the real part. To quantify this, we consider the logarithmic plots: here we observe that the (absolute value of the) imaginary part is typically a few orders of magnitude smaller than the real part. This continues also to large spins. The only exceptions are the amplitudes which almost vanish, where the Monte Carlo method suffers from the sign problem. Here real and imaginary part are of a similar magnitude and it is likely that neither has converged for the given samples. Thus, in most cases, we reproduce a significantly smaller imaginary part, but far away from the limits of numerical accuracy. It is clear that more samples are necessary to further improve the imaginary part, yet we suspect it might give diminishing returns due to the sign problem. At least for the coherent vertex amplitude, this level of accuracy appears acceptable.

As the final plot for the equilateral 4-simplex, we show the relative error of the real part in fig. 7. For small spins, the relative error from importance sampling is comparable to the random sampling results for ten times the samples, and the relative error is below 1% in most cases. For large spins compared to the asymptotic formula, we see again more randomness, but most errors are below 10%. Considering the size of the boundary spins this is an impressively accurate result, but it also shows that more samples are necessary to obtain a more precise result.

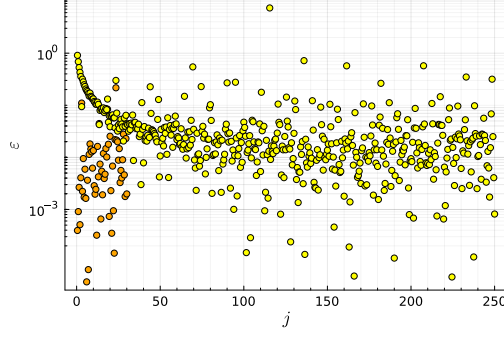


Figure 7: Relative error ϵ of real part of amplitude with respect to the full vertex amplitude calculation (orange) and its asymptotic approximation (yellow) for spins $j = 0.5$ to 250.

4.2.2 Isosceles 4-simplex

An isosceles 4-simplex possesses only two different edge lengths, four of its edges have one lengths, the remaining six the other. The latter six edges form an equilateral tetrahedron. All remaining tetrahedra are isosceles, i.e. they have an equilateral triangle as their base and the three remaining edges have equal lengths different from the base triangle. Here, we consider an isosceles tetrahedron, whose equilateral triangles have twice the area of the isosceles ones. To do so, we assign the following boundary data: first, we label the equilateral tetrahedron as 5, whereas $i \in \{1, 2, 3, 4\}$ denote isosceles tetrahedra. Thus, the spins are:

$$j_{ab} = j \quad \forall a, b < 5, a \neq b, \quad j_{a5} = 2j \quad \forall a \neq 5 \quad . \quad (4.6)$$

The smallest non-vanishing spin we can start from is $j = 1$. Non-integer spins are violating the $SU(2)$ coupling rules in the isosceles tetrahedra. We assign the following normal vectors: For the equilateral 4-simplex, we again assign the data for equilateral tetrahedra, see eq. Eq. (4.5). The new data is for the isosceles tetrahedra:

$$\begin{aligned} \vec{n}_{12} &= (0, 0, 1) \quad , \quad \vec{n}_{13} = \left(0, 0.9860, \frac{1}{6}\right) \quad , \\ \vec{n}_{14} &= \left(0.9759, 0.14086, \frac{1}{6}\right) \quad , \quad \vec{n}_{15} = \left(-0.48795, -0.5635, -\frac{2}{3}\right) \quad . \end{aligned} \quad (4.7)$$

The last vector is the one assigned to the equilateral triangle with twice the area compared to the isosceles one. Again, we are not using a twisted spike configuration.

Results As for the equilateral case, we consider 30 runs with 10^5 samples. The results including comparison to the full and asymptotic amplitude can be found in fig. 8, where we plot the results over the scaling parameter λ , $(j, 2j) \rightarrow (\lambda j, 2\lambda j)$, up to $\lambda = 125$. Since the results are qualitatively similar to the equilateral 4-simplex case, we keep the discussion brief.

Let us begin with the plots of the rescaled amplitude, where we observe a good agreement to the full amplitude, small variances and small imaginary part close to zero. For $\lambda > 35$ we compare to the asymptotic approximation, which is closely but not fully matched

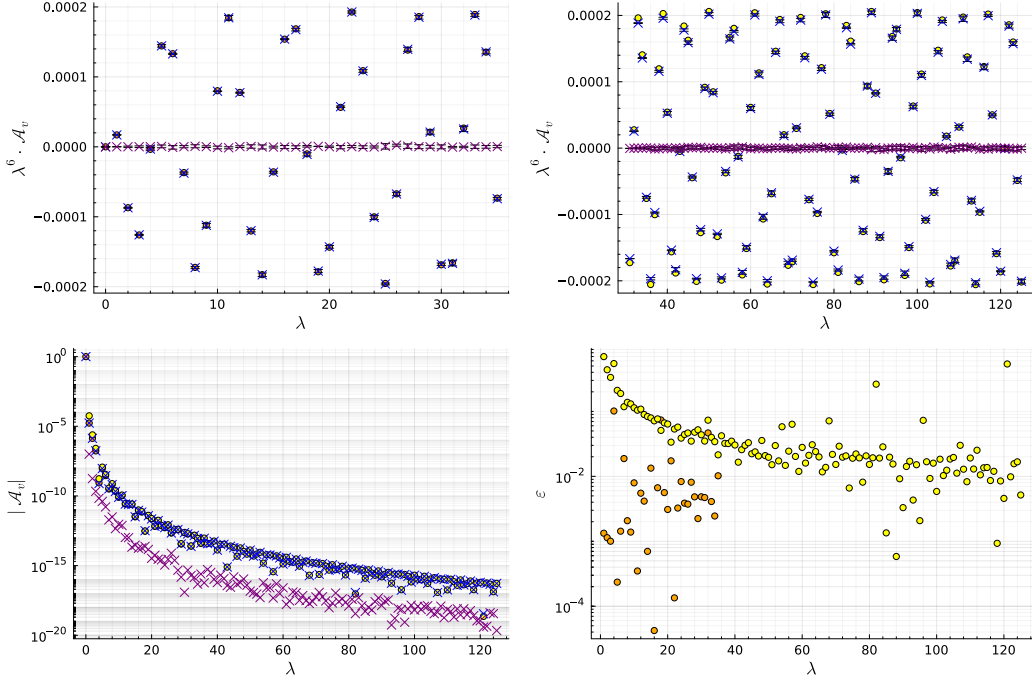


Figure 8: Importance sampling results for the isosceles case. *Top left:* rescaled amplitude compared to full calculation up to $\lambda = 35$. *Top right:* rescaled amplitude compared to asymptotic formula up to $\lambda = 125$. *Bottom left:* logarithmic plot of absolute value of real and imaginary part and comparison to full and asymptotic vertex amplitude. *Bottom right:* relative error with respect to full and asymptotic amplitude.

for $\lambda < 60$. This might be because the asymptotic approximation is not good enough yet, and the matching improves for larger λ . In the logarithmic plot, we can barely see any deviations. For the isosceles 4-simplex, we observe only few boundary data for which the coherent amplitude almost vanishes, thus we encounter less cases suffering from a severe sign problem leading to convergence issues. Additionally, the logarithmic plots show similar to the equilateral case that the imaginary part is a few orders of magnitude smaller than the real one, but not vanishing completely (or to numerical precision). The precision of the real part is confirmed by the relative error of the (real part of the) amplitude. Compared to the full calculation, the error is below 1%, except for one case where the amplitude is small. For the asymptotic formula, the relative error drops quickly and appears to asymptote to below 10% for large λ , which shows the convergence of the asymptotic formula to the full one. Due to the randomness of Monte Carlo method, we see fluctuations of this error.

4.2.3 Non-regular 4-simplex

The next example is an irregular 4-simplex, which possesses two different triangle areas, namely j and $2j$, but these are not assigned to form an isosceles 4-simplex, but a non-regular configuration. For $j = 1$, this 4-simplex is prescribed by three different edge lengths: $l_1 \approx 1.58$, $l_2 \approx 2.74$ and $l_3 \approx 1.52$. One of its five tetrahedra is equilateral with edge length l_3 , one is isosceles with base length l_3 and l_2 as the other length. The three

remaining tetrahedra have one equilateral, one isosceles and two non-regular triangles, where the remaining edge has length l_1 . In the following we specify the five tetrahedra in terms of their spin foam boundary data (not in a twisted spike configuration) and add the edge lengths as further information. To keep the notation consistent with the numbering of tetrahedra, we label the edge lengths by the set of three tetrahedra sharing it in the 4-simplex.

Tetrahedron 1 - non-regular:

$$\begin{aligned}
l_{134} &= l_1, & l_{123} &= l_{124} = l_2, & l_{125} &= l_{135} = l_{145} = l_3 \quad . \\
j_{12} &= 2j \quad , & \vec{n}_{12} &= (0, 0, 1) \quad , \\
j_{13} &= j \quad , & \vec{n}_{13} &= (0, 0.83099, -0.55629) \quad , \\
j_{14} &= j & \vec{n}_{14} &= (0.44287, -0.70315, -0.55629) \quad , \\
j_{15} &= j \quad , & \vec{n}_{15} &= (-0.44287, -0.12784, -0.88743) \quad . \tag{4.8}
\end{aligned}$$

Tetrahedron 2 - isosceles:

$$\begin{aligned}
l_{123} &= l_{124} = l_{234} = l_2, & l_{125} &= l_{235} = l_{245} = l_3 \quad . \\
j_{12} &= 2j \quad , & \vec{n}_{21} &= (0, 0, 1) \quad , \\
j_{23} &= 2j \quad , & \vec{n}_{23} &= (0, 0.88878, -0.458333) \quad , \\
j_{24} &= 2j & \vec{n}_{24} &= (0.473665, -0.75204, -0.458333) \quad , \\
j_{25} &= j \quad , & \vec{n}_{25} &= (-0.94733, -0.27347, -0.16667) \quad . \tag{4.9}
\end{aligned}$$

Tetrahedron 3 - non-regular:

$$\begin{aligned}
l_{134} &= l_1, & l_{123} &= l_{234} = l_2, & l_{135} &= l_{235} = l_{345} = l_3 \quad . \\
j_{13} &= j \quad , & \vec{n}_{31} &= (0, 0, 1) \quad , \\
j_{23} &= 2j \quad , & \vec{n}_{32} &= (0, 0.83099, -0.55629) \quad , \\
j_{34} &= j & \vec{n}_{34} &= (0.44287, -0.85342, -0.27485) \quad , \\
j_{35} &= j \quad , & \vec{n}_{35} &= (-0.44287, -0.80856, 0.38743) \quad . \tag{4.10}
\end{aligned}$$

Tetrahedron 4 - non-regular:

$$\begin{aligned}
l_{134} &= l_1, & l_{124} &= l_{234} = l_2, & l_{145} &= l_{245} = l_{345} = l_3 \quad . \\
j_{14} &= j \quad , & \vec{n}_{41} &= (0, 0, 1) \quad , \\
j_{24} &= 2j \quad , & \vec{n}_{42} &= (0, 0.83099, -0.55629) \quad , \\
j_{34} &= j & \vec{n}_{43} &= (0.44287, -0.85342, -0.27485) \quad , \\
j_{45} &= j \quad , & \vec{n}_{45} &= (-0.44287, -0.80856, 0.38743) \quad . \tag{4.11}
\end{aligned}$$

Tetrahedron 5 - equilateral:

$$l_{125} = l_{135} = l_{235} = l_{145} = l_{245} = l_{345} = l_3 \quad .$$

$$j_{15} = j \quad , \quad \vec{n}_{51} = (0, 0, 1) \quad ,$$

$$j_{25} = j \quad , \quad \vec{n}_{52} = \left(0, 0.94281, -\frac{1}{3}\right) \quad ,$$

$$j_{35} = j \quad \vec{n}_{53} = \left(0.8165, -0.47141, -\frac{1}{3}\right) \quad ,$$

$$j_{45} = j \quad , \quad \vec{n}_{54} = \left(-0.8165, -0.47141, -\frac{1}{3}\right) \quad . \quad (4.12)$$

Results The results for the non-regular 4-simplex are summarised in fig. 9. All plots are over λ , which scales all spins according to $(j, 2j) \rightarrow (\lambda j, \lambda 2j)$. Beginning with the plots of the rescaled amplitude, we observe again a very good agreement of the (real part of the) Monte Carlo simulations with the full coherent vertex amplitude up to $\lambda = 30$. For $\lambda > 30$ we compare to the asymptotic formula, where the results initially deviate slightly from the asymptotic formula and the agreement improves under increasing λ . Again, this signifies convergence of the asymptotic formula to the full result. For all values of λ tested, namely up to $\lambda = 120$, the margins indicating the variance of the runs remain small. More importantly, the imaginary part, which is supposed to vanish, is small also with small error estimates. These findings are confirmed in the logarithmic plots, where we essentially see no deviations for the real part; it seems for the boundary data considered we do not encounter a severe sign problem and observe convergence for the used number of samples. Moreover, the imaginary part is again a few orders of magnitude smaller than the real part. Lastly, the relative error is also fairly low: for the full computation it is below 1% in most cases ($\lambda < 30$), while the relative error for the asymptotic formula asymptotes to a level fairly below 10%.

4.3 Computational time

Besides the accuracy of the algorithm, we must discuss the computational costs and compare them to existing algorithms, in particular the full calculation utilizing tensor network techniques. Already, we can infer that the Monte Carlo simulations are more efficient due to the fact that we could perform simulations for significantly larger values of boundary spins. Indeed, there are two limiting factors for the full calculation, memory and computational time. In an effort to reduce the computational time, tensor network methods, e.g. implemented in Julia in the package `TensorOperations`¹¹, utilize linear algebra techniques that are highly optimized, fast and can additionally utilize graphics processors (GPUs) for further acceleration. However, this comes with higher memory costs, e.g. for the coherent vertex amplitude we must store a five dimensional array storing all possible values of the $\{15j\}$ -symbol, and can quickly go beyond the capabilities of consumer hardware¹². Here

¹¹<https://jutho.github.io/TensorOperations.jl/stable/>

¹²In particular memory costs can be optimized by rewriting a problem in terms of tensors with less indices. In general this also improves computational time and helps in adapting code to GPUs, which typically have more limited memory. Such an optimization for coherent vertex amplitudes is promising.

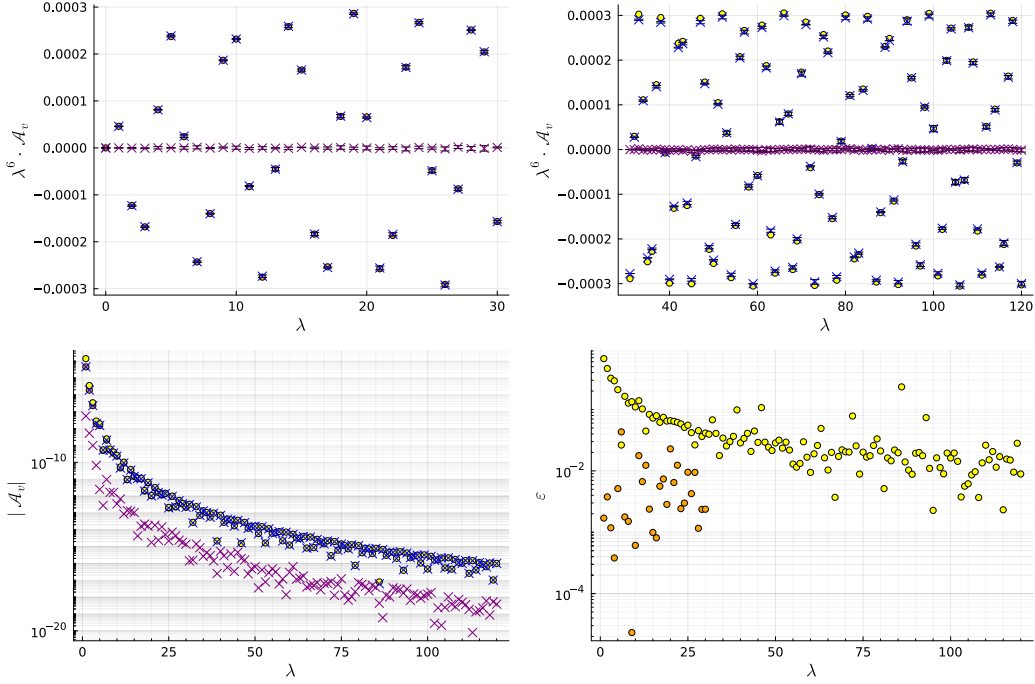


Figure 9: Importance sampling results for the non-regular case. *Top left:* rescaled amplitude compared to full calculation up to $\lambda = 30$. *Top right:* rescaled amplitude compared to asymptotic formula up to $\lambda = 120$. *Bottom left:* logarithmic plot of absolute value of real and imaginary part and comparison to full and asymptotic vertex amplitude. *Bottom right:* relative error with respect to full and asymptotic amplitude.

instead, our main focus is on the computational time and we will try to compare the Monte Carlo simulations to a fast current algorithm.

We measure all computational times on a desktop computer equipped with an Intel® Core™ i5-10400 and 32 GB of memory. To measure the computational time and avoid other influences like compilation time, we have used **BenchmarkTools** in **Julia**. To have a better comparison between the algorithms that specifically compute the vertex amplitude, we have precomputed (and benchmarked the computation of) the coherent states as well. For the Monte Carlo algorithm, we show the result for a single run with 10^5 and 10^6 samples (each with 10^4 thermalization steps and 10^3 steps between taking samples). The data shown in fig. 10 are for an equilateral 4-simplex.

As already suspected in sec. 2, the full calculation clearly outperforms the Monte Carlo algorithms at small spins ($j \leq 10$). Recall that the number of intertwiners to sum over is $(2j + 1)^5$ in this case, which is lower than or of a similar size as the number of samples used in the Monte Carlo algorithm. We could have lowered the number of samples to make the Monte Carlo algorithm more efficient, yet since the full calculation is fast and accurate in this regime, there is not reason to use Monte Carlo methods. The situation rapidly changes for $j > 10$, as the numerical costs for the full calculation grow exponentially and the Monte Carlo algorithm becomes more efficient. From the double-logarithmic plot we also see that the numerical costs of the Monte Carlo algorithm grow linearly with the

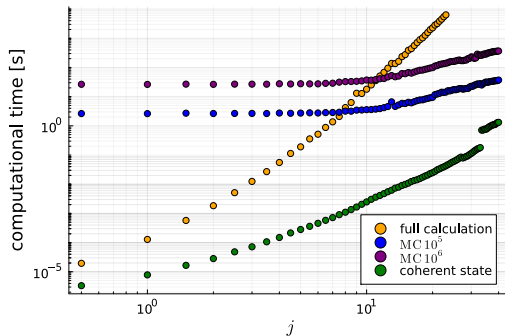


Figure 10: Computational time in seconds plotted over the spin j . Measurements for equilateral coherent amplitude / coherent state respectively.

number of samples, indicated by the linear shift. Note also that changing the number of thermalization steps and number of steps between samples will have an impact on the numerical costs. Moreover, the numerical costs of the Monte Carlo algorithms grow with growing spins. This is because the evaluation of $\{15j\}$ -symbols becomes more costly as the range of the sum over internal auxiliary spins in eq. (2.2) grows linearly under uniformly scaling the spins.

Despite this level of efficiency, we cannot use the Monte Carlo algorithm to go to arbitrarily high boundary spins. First, the computational costs grow with growing boundary spins. Second, with higher intertwiner ranges, we expect that we must increase the number of samples further, too. Lastly, increasing the boundary spins has revealed another source of computational complexity, the coherent states. As we can see from fig. 10, the time to calculate a coherent states grows rapidly with growing boundary spins. It is defined as a sum over three magnetic indices, the fourth being fixed as a function of the remaining three, of four Wigner matrices and a $4jm$ -symbol, see eq. (2.7). Since the range of magnetic indices grows with the size of the spin, the costs scale rapidly, but dwarf compared to the costs of the full calculation. Eventually, analytical methods such as asymptotic expansions should be accurate enough and more efficient to compute in such large spin regimes. As we have seen, Monte Carlo methods can bridge this gap between the full calculation and asymptotic formulae for a single vertex, and the gained efficiency can be used to explore larger 2-complexes.

5 Discussion and conclusion

Markov Chain Monte Carlo methods are a powerful tool to explore the dynamics of high dimensional statistical theories. To do so, one uses the partition function to sample probable configurations and approximate expectation values of observables. The same strategy cannot be applied to spin foams, as the amplitudes are typically complex. Thus, we cannot directly use the partition function to define a probability distribution for sampling, and we must propose a new one. Yet, even if we do so, due to the oscillatory nature of the amplitudes, the results might not converge, which is known as the sign problem. However, we do not know yet how severe this sign problem is.

In this article we propose a probability distribution for sampling intertwiners derived from coherent states, concretely coherent (space-like) tetrahedra, which can be straightforwardly applied to coherent boundary data of spin foams. The idea is to sample with respect to the absolute value of the coefficient of the coherent states expressed in the orthonormal spin network basis. For large spins and coherent tetrahedra, this is a function of one intertwiner label and sharply peaked. The distribution is defined independently for each tetrahedron, and hence can be directly generalized to boundaries with arbitrarily many boundary tetrahedra. We then use this distribution to approximate the so-called coherent vertex amplitude for a 4-simplex, where we sample the data from its five boundary tetrahedra.

We perform this study in $SU(2)$ BF theory for three different sets of Regge-type boundary data, an equilateral, an isosceles and a non-regular Euclidean 4-simplex and compare the approximation to the full numerical calculation and the asymptotic formula. It is best to separately discuss the real and imaginary part of the amplitude. For the real part, we observe for almost all cases an excellent agreement to the full calculation and at sufficiently large spins to the asymptotic formula already at a moderate sample size. These results are very encouraging for two reasons: first, the results are obtained at substantially lower numerical costs compared to the full numerical calculation, which allows us to instead increase the size of the boundary spins by almost an order of magnitude. Second, the fact that the results have converged to the known results at a moderate number of samples suggests that the sign problem is not severe in these cases, at least for the real part in most cases. However, as the coherent amplitude oscillates with the Regge action under uniform scaling of the boundary spins, some amplitudes almost vanish. In these cases, the sign problem is more severe: the various terms summed over cancel almost completely, which is difficult to capture using Monte Carlo sampling methods.

In contrast to the real part, the sign problem is present in the imaginary part for all boundary data. This is the case for our choice of global phase, which renders the full amplitude purely real¹³. Therefore, the imaginary part always vanishes by definition, i.e. the various imaginary parts of summands exactly cancel. Again, this sign problem is challenging for Monte Carlo algorithms, yet for the cases studied the imaginary part is usually a few orders of magnitude smaller than the real part. An exception are the cases where the entire amplitude is small (compared to boundary data of similar size). Moreover, we observe that convergence of the imaginary part is worse for larger boundary spins, but still under control. We expect that this can be improved by increasing the number of samples, yet it is not clear how efficient this is.

In terms of computational costs, the full calculation is only more efficient for small spins. Above spins of the order 10 the costs grow so rapidly that the Monte Carlo method quickly becomes more efficient and provides an accurate approximation. Hence, it should be possible to use the freed resources for simulations of larger boundary spins and bridge the gap to the asymptotic approximations. The good accuracy is also an advantage of

¹³This phase choice is convenient for demonstrating the sign problem. For other choices the sign problem manifests itself by the difficulty of determining the phase. Recall that we have used the phase from the full calculation and scaled it with the spins.

the importance sampling algorithm compared to randomly sampling coherent intertwiners. Random sampling provides decent and convergent results for real and imaginary parts, but requires more samples to do so. Additionally, the number of samples required to obtain a convergent results grow with growing boundary spins. Still random sampling is useful for sampling bulk spins and intertwiners [31].

To sum up, sampling coherent intertwiners using Monte Carlo techniques is efficient and accurate at simulating the coherent $SU(2)$ BF vertex amplitude. This is an important proof of principle and opens the door for more efficient studies of spin foams defined on larger 2-complexes and for larger boundary spins, such that we can better bridge the gap between the full calculation and asymptotic approximations, the latter e.g. via the complex critical points method [19, 20].

5.1 Generalizing the algorithm

In the following, we discuss several directions in which the algorithm can be generalized, namely to larger 2-complexes, to the Lorentzian EPRL model and sampling bulk intertwiners.

Larger 2-complexes with boundary If the boundary states for spin foams defined on larger 2-complexes are given by coherent states, the algorithm presented in this article can be straightforwardly generalized to this setting. The probability distribution is defined individually for each intertwiner, i.e. they are explicitly independent from one another. Hence, this method can be extended to almost arbitrarily many coherent boundary tetrahedra. Of course, more boundary intertwiners readily imply increased numerical costs alone for computing coherent states (and the normalization to define the probability distribution). More importantly, more degrees of freedom generically require larger numbers of samples to obtain convergent results. Obviously, the same is true for the full calculation and, as is typical for Monte Carlo methods, we expect our algorithm to more beneficially scale with the size of the system and the size of boundary spins.

So far we have left bulk variables, i.e. representations and bulk intertwiners, undressed. The most direct option is to sum over these variables, yet this becomes inefficient quickly: if we have N samples for all boundary data combined, we must sum over all bulk variables N times. This is probably still more efficient than summing over all data exactly, but loses the beneficial scaling of Monte Carlo algorithms. Instead, one can use random sampling for the bulk variables as in [31].

Lorentzian (and Riemannian) EPRL coherent vertex amplitude BF theory written in the spin foam representation is computationally non-trivial, simpler than modern 4d spin foam models, yet similar enough to those models for methods to be transferable. Indeed, both the Riemannian and Lorentzian EPRL models use coherent states derived from the same $SU(2)$ boundary states. More precisely, the same coefficients $c_i(\{j_i\}, \{\vec{n}_i\})$ appear in the coherent amplitudes, see e.g. the derivation for the Lorentzian model in the seminal paper by Speziale [91]. Hence, the sampling algorithm should be straightforwardly applicable, where one has to replace the $SU(2)$ $\{15j\}$ -symbol by the appropriate $\text{Spin}(4)$ / $\text{SL}(2, \mathbb{C})$ vertex amplitude with orthonormal boundary spin network data. Computing said

amplitude is computationally non-trivial, in particular for the Lorentzian model [27, 32]. Therefore, the here presented algorithm might be highly beneficial for the Lorentzian case, if it helps approximate coherent amplitudes with fewer samples.

Sampling bulk intertwiners Given the good convergence of the algorithm presented here, the question arises whether this method can also be applied to bulk variables. The following considerations are more speculative, but we believe this method to have potential there as well.

Without the boundary, we clearly cannot rely on external data to choose a probability distribution. Instead we have to guess one and at best it should be one adapted to the dynamics of the system we are considering. Already for the boundary, the coherent states work best as the spins are larger and one approaches the asymptotic regime of the vertex amplitude [12–14, 67]. For a single vertex amplitude, asymptotic analysis informs us for which boundary data the amplitude possesses critical points and thus which amplitudes dominate in the large spin limit. Hence, it might be possible to use the information of critical points in turn to guess a probability distribution for bulk intertwiners.

However this is easier said than done. Typically, there exist two types of solutions to the critical point equations for a single 4-simplex, Regge geometries and so-called vector geometries [12–16, 67]. The former have two inequivalent critical points, giving rise to the characteristic oscillations of the amplitude with the Regge action, while the latter only have one. For our considerations more relevant is the fact that Regge geometries span a 10-dimensional space in the boundary Hilbert space of a 4-simplex, while vector geometries span a 15-dimensional space [26]. Indeed, for fixed spins a Regge geometry corresponds to an isolated point in that space, whereas vector geometries span an intricate 5-dimensional space of configurations and are not isolated, i.e. one can continuously vary the parameters and obtain another vector geometry. Hence, it is unrealistic to guess a probability distribution for bulk intertwiners taking all critical configurations into account.

Instead, one can entertain the thought to devise a probability distribution defined only from Regge geometries of the vertices. For fixed spins, we determine the Regge critical points by looking for length configurations of flat simplices compatible with the assigned areas [45, 92]. There can be multiple configurations fulfilling these requirements. For these Regge geometries, we can compute the spin foam boundary data for each of the tetrahedra and derive a probability distribution from their coherent states. In case there are multiple Regge critical points, we can choose one, e.g. as it best fits prescribed boundary data; most general would be to consider a superposition of the critical coherent states. However, so far we have only considered the information from one vertex, yet each bulk edge is shared by two vertices. Therefore we propose to use a (suitably normalized) product of distributions, which is informed by both vertices. This could lead to situations, where the critical points associated to the two vertices do not agree and the coherent states describe non-matching tetrahedra. Hence, the algorithm would mostly sample intertwiners where the distributions overlap, which however do not fit well with neither critical point(s) and would lead to an exponential suppression. Such scenarios strongly resonate with the ideas of gluing constraints introduced in effective spin foams [38, 93] and computed for spin foams

models in the context of a hybrid algorithm [41].

This idea has a few drawbacks. For the numerical implementation, there are two challenges. The first one is to compute the Regge geometries for various spin assignments, the spin foam boundary data and the coherent states. Indeed, we have seen that the latter can become costly for large spins as well. Second, even though we would then sample over intertwiners, the sum over bulk spins is unaddressed. Thus, one has to repeat this procedure and then sample for each spin assignment in the bulk. Besides these practical considerations, this choice represents also a substantial truncation of the spin foam partition function as we are excluding many bulk intertwiner degrees of freedom. We expect that some of these will play a role in the asymptotic regime as vector geometries. Conversely, this setup allows us to investigate the relevance of vector geometries in the partition function, e.g. whether they are suppressed for geometric boundary data in larger complexes. Moreover, in the Lorentzian theory we can choose to only sample Regge boundary data for critical points corresponding to Lorentzian 4-simplices, i.e. exclude vector geometries including those Euclidean Regge geometric boundary data [14, 27]. In a way, its underlying idea is similar to effective spin foams [38, 93], but implemented in the full theory. Thus, a comparison to this method as well as complex critical points [19, 20] would be interesting.

Closing remarks To conclude, we have presented an algorithm that samples boundary intertwiners according to their associated coherent boundary data. For the example of the $SU(2)$ coherent vertex amplitude considered here it offers a good approximation at much lower numerical costs compared to the full numerical calculation and is able to bridge the gap to the regime where the asymptotic formula is valid. It is straightforward to generalize this to larger 2-complexes / triangulations with boundary. While the sign problem is present, it is under control in the vast majority of cases and must results show a good convergence. Therefore, we are optimistic that the algorithm scales well for more degrees of freedom and can additionally be generalized to the Lorentzian EPRL model. We also suggest an application to bulk intertwiners, which however corresponds to a big truncation excluding vector geometries and must be justified. What is still missing is a dynamics informed method to sample bulk representations. We leave these specific questions and developments to further optimize spin foam numerics for future research.

Acknowledgements

The author would like to thank Seth Asante, José Simão, Alexander Jercher, Pietro Donà, L Glaser and Kevin Siebert for fruitful discussions and clarifying questions. The author also gratefully acknowledges access to the Ara-Cluster at FSU Jena, which was used to produce most of the numerical results presented in this article.

The author gratefully acknowledges support by the Deutsche Forschungsgemeinschaft (DFG, German Research Foundation) project number 422809950.

References

- [1] A. Pérez, *The Spin-Foam Approach to Quantum Gravity*, *Living Rev. Relativity* **16** (2013) 3 [[1205.2019](#)].
- [2] J. Engle and S. Speziale, *Spin Foams: Foundations*, Springer (2023), DOI [[2310.20147](#)].
- [3] C. Rovelli, *Quantum Gravity*, Cambridge University Press, Cambridge, UK (2004).
- [4] T. Thiemann, *Modern canonical quantum general relativity*, Cambridge University Press, Cambridge, UK (2007).
- [5] J.C. Baez and J.W. Barrett, *The Quantum tetrahedron in three-dimensions and four-dimensions*, *Adv. Theor. Math. Phys.* **3** (1999) 815 [[gr-qc/9903060](#)].
- [6] J.C. Baez, *An Introduction to Spin Foam Models of BF Theory and Quantum Gravity*, in *Geometry and Quantum Physics*, (Berlin, Heidelberg), pp. 25–93, Springer (2000) [[gr-qc/9905087](#)].
- [7] J.F. Plebanski, *On the Separation of Einsteinian Substructures*, *J. Math. Phys.* **18** (1977) 2511.
- [8] B. Dittrich, *The Continuum Limit of Loop Quantum Gravity: A Framework for Solving the Theory*, in *Loop Quantum Gravity*, A. Ashtekar, ed., 100 Years of General Relativity, pp. 153–179, World Scientific (2017) [[1409.1450](#)].
- [9] S. Steinhaus, *Coarse Graining Spin Foam Quantum Gravity—A Review*, *Front. in Phys.* **8** (2020) 295 [[2007.01315](#)].
- [10] S.K. Asante, B. Dittrich and S. Steinhaus, *Spin foams, Refinement limit and Renormalization*, Springer (2022), DOI [[2211.09578](#)].
- [11] E.R. Livine and S. Speziale, *New spinfoam vertex for quantum gravity*, *Phys. Rev. D* **76** (2007) 084028 [[0705.0674](#)].
- [12] F. Conrady and L. Freidel, *On the semiclassical limit of 4d spin foam models*, *Phys. Rev. D* **78** (2008) 104023 [[0809.2280](#)].
- [13] J.W. Barrett, R.J. Dowdall, W.J. Fairbairn, H. Gomes and F. Hellmann, *Asymptotic analysis of the Engle-Pereira-Rovelli-Livine four-simplex amplitude*, *J. Math. Phys.* **50** (2009) 2504 [[0902.1170](#)].
- [14] J.W. Barrett, R.J. Dowdall, W.J. Fairbairn, F. Hellmann and R. Pereira, *Lorentzian spin foam amplitudes: Graphical calculus and asymptotics*, *Class. Quant. Grav.* **27** (2010) 165009 [[0907.2440](#)].
- [15] W. Kaminski, M. Kisielowski and H. Sahlmann, *Asymptotic analysis of the EPRL model with timelike tetrahedra*, *Class. Quant. Grav.* **35** (2018) 135012 [[1705.02862](#)].
- [16] H. Liu and M. Han, *Asymptotic analysis of spin foam amplitude with timelike triangles*, *Phys. Rev. D* **99** (2019) 084040 [[1810.09042](#)].
- [17] J.D. Simão and S. Steinhaus, *Asymptotic analysis of spin-foams with timelike faces in a new parametrization*, *Phys. Rev. D* **104** (2021) 126001 [[2106.15635](#)].
- [18] T.E. Regge, *General relativity without coordinates*, *Nuovo Cimento* **19** (1961) 558.
- [19] M. Han, Z. Huang, H. Liu and D. Qu, *Complex critical points and curved geometries in four-dimensional Lorentzian spinfoam quantum gravity*, *Phys. Rev. D* **106** (2022) 044005 [[2110.10670](#)].

- [20] M. Han, H. Liu and D. Qu, *Complex critical points in Lorentzian spinfoam quantum gravity: Four-simplex amplitude and effective dynamics on a double- Δ^3 complex*, *Phys. Rev. D* **108** (2023) 026010 [[2301.02930](#)].
- [21] M. Han, H. Liu, D. Qu, F. Vidotto and C. Zhang, *Cosmological Dynamics from Covariant Loop Quantum Gravity with Scalar Matter*, [2402.07984](#).
- [22] P. Dona, M. Han and H. Liu, *Spinfoams and high performance computing*, Springer (2022) [[2212.14396](#)].
- [23] F. Hellmann and W. Kaminski, *Holonomy spin foam models: Asymptotic geometry of the partition function*, *JHEP* **10** (2013) 165 [[1307.1679](#)].
- [24] J.S. Engle, W. Kaminski and J.R. Oliveira, *Addendum to ‘EPRL/FK asymptotics and the flatness problem’*, [2012.14822](#).
- [25] J. Engle and C. Rovelli, *The accidental flatness constraint does not mean a wrong classical limit*, *Class. Quant. Grav.* **39** (2022) 117001 [[2111.03166](#)].
- [26] P. Dona, M. Fanizza, G. Sarno and S. Speziale, *$SU(2)$ graph invariants, Regge actions and polytopes*, *Class. Quant. Grav.* **35** (2018) 045011 [[1708.01727](#)].
- [27] P. Dona, M. Fanizza, G. Sarno and S. Speziale, *Numerical study of the Lorentzian Engle-Pereira-Rovelli-Livine spin foam amplitude*, *Phys. Rev. D* **100** (2019) 106003 [[1903.12624](#)].
- [28] P. Dona and P. Frisoni, *How-to Compute EPRL Spin Foam Amplitudes*, *Universe* **8** (2022) 208 [[2202.04360](#)].
- [29] P. Donà, F. Gozzini and G. Sarno, *Numerical analysis of spin foam dynamics and the flatness problem*, *Phys. Rev. D* **102** (2020) 106003 [[2004.12911](#)].
- [30] P. Donà, P. Frisoni and E. Wilson-Ewing, *Radiative corrections to the Lorentzian Engle-Pereira-Rovelli-Livine spin foam propagator*, *Phys. Rev. D* **106** (2022) 066022 [[2206.14755](#)].
- [31] P. Donà and P. Frisoni, *Summing bulk quantum numbers with Monte Carlo in spin foam theories*, *Phys. Rev. D* **107** (2023) 106008 [[2302.00072](#)].
- [32] F. Gozzini, *A high-performance code for EPRL spin foam amplitudes*, *Class. Quant. Grav.* **38** (2021) 225010 [[2107.13952](#)].
- [33] J. Engle, E.R. Livine, R. Pereira and C. Rovelli, *LQG vertex with finite Immirzi parameter*, *Nucl. Phys. B* **799** (2008) 136 [[0711.0146](#)].
- [34] L. Freidel and K. Krasnov, *A new spin foam model for 4D gravity*, *Class. Quant. Grav.* **25** (2008) 125018 [[0708.1595](#)].
- [35] G. Sarno, S. Speziale and G.V. Stagno, *2-vertex Lorentzian Spin Foam Amplitudes for Dipole Transitions*, *Gen. Rel. Grav.* **50** (2018) 43 [[1801.03771](#)].
- [36] P. Frisoni, F. Gozzini and F. Vidotto, *Markov chain Monte Carlo methods for graph refinement in spinfoam cosmology*, *Class. Quant. Grav.* **40** (2023) 105001 [[2207.02881](#)].
- [37] P. Frisoni, *Numerical approach to the black-to-white hole transition*, *Phys. Rev. D* **107** (2023) 126012 [[2304.02691](#)].
- [38] S.K. Asante, B. Dittrich and H.M. Haggard, *Effective Spin Foam Models for Four-Dimensional Quantum Gravity*, *Phys. Rev. Lett.* **125** (2020) 231301 [[2004.07013](#)].

- [39] S.K. Asante, B. Dittrich and H.M. Haggard, *Discrete gravity dynamics from effective spin foams*, *Class. Quant. Grav.* **38** (2021) 145023 [[2011.14468](#)].
- [40] S.K. Asante, B. Dittrich and J. Padua-Argüelles, *Complex actions and causality violations: applications to Lorentzian quantum cosmology*, *Class. Quant. Grav.* **40** (2023) 105005 [[2112.15387](#)].
- [41] S.K. Asante, J.D. Simão and S. Steinhaus, *Spin-foams as semiclassical vertices: Gluing constraints and a hybrid algorithm*, *Phys. Rev. D* **107** (2023) 046002 [[2206.13540](#)].
- [42] B. Dittrich and J. Padua-Argüelles, *Lorentzian quantum cosmology from effective spin foams*, [2306.06012](#).
- [43] J.W. Barrett, M. Rocek and R.M. Williams, *A note on area variables in Regge calculus*, *Class. Quant. Grav.* **16** (1999) 1373 [[gr-qc/9710056](#)].
- [44] B. Dittrich and S. Speziale, *Area-angle variables for general relativity*, *New J. Phys.* **10** (2008) 083006 [[0802.0864](#)].
- [45] S.K. Asante, B. Dittrich and H.M. Haggard, *The Degrees of Freedom of Area Regge Calculus: Dynamics, Non-metricity, and Broken Diffeomorphisms*, *Class. Quant. Grav.* **35** (2018) 135009 [[1802.09551](#)].
- [46] R.G. Liu and R.M. Williams, *Regge calculus models of the closed vacuum Λ -FLRW universe*, *Phys. Rev. D* **93** (2016) 024032 [[1501.07614](#)].
- [47] B. Dittrich, S. Gielen and S. Schander, *Lorentzian quantum cosmology goes simplicial*, *Class. Quant. Grav.* **39** (2022) 035012 [[2109.00875](#)].
- [48] A.F. Jercher and S. Steinhaus, *Cosmology in Lorentzian Regge calculus: causality violations, massless scalar field and discrete dynamics*, [2312.11639](#).
- [49] B. Dittrich and A. Kogios, *From spin foams to area metric dynamics to gravitons*, [2203.02409](#).
- [50] R. Schmidt, *Xxxii. on the numerical solution of linear simultaneous equations by an iterative method*, *The London, Edinburgh, and Dublin Philosophical Magazine and Journal of Science* **32** (1941) 369 [<https://doi.org/10.1080/14786444108520797>].
- [51] D. Shanks, *Non-linear transformations of divergent and slowly convergent sequences*, *Journal of Mathematics and Physics* **34** (1955) 1 [<https://onlinelibrary.wiley.com/doi/pdf/10.1002/sapm19553411>].
- [52] B. Bahr and S. Steinhaus, *Investigation of the Spinfoam Path integral with Quantum Cuboid Intertwiners*, *Phys. Rev. D* **93** (2016) 104029 [[1508.07961](#)].
- [53] B. Bahr, S. Klöser and G. Rabuffo, *Towards a Cosmological subsector of Spin Foam Quantum Gravity*, *Phys. Rev. D* **96** (2017) 086009 [[1704.03691](#)].
- [54] M. Assanioussi and B. Bahr, *Hopf link volume simplicity constraints in spin foam models*, *Class. Quant. Grav.* **37** (2020) 205003 [[2005.12004](#)].
- [55] B. Bahr and S. Steinhaus, *Numerical Evidence for a Phase Transition in 4D Spin-Foam Quantum Gravity*, *Phys. Rev. Lett.* **117** (2016) [[1605.07649](#)].
- [56] B. Bahr and S. Steinhaus, *Hypercuboidal renormalization in spin foam quantum gravity*, *Phys. Rev. D* **95** (2017) 126006 [[1701.02311](#)].

- [57] B. Bahr, G. Rabuffo and S. Steinhaus, *Renormalization of symmetry restricted spin foam models with curvature in the asymptotic regime*, *Phys. Rev. D* **98** (2018) 106026 [[1804.00023](#)].
- [58] S. Steinhaus and J. Thürigen, *Emergence of Spacetime in a restricted Spin-foam model*, *Phys. Rev. D* **98** (2018) 026013 [[1803.10289](#)].
- [59] A.F. Jercher, S. Steinhaus and J. Thürigen, *Curvature effects in the spectral dimension of spin foams*, *Phys. Rev. D* **108** (2023) 066011 [[2304.13058](#)].
- [60] M. Ali and S. Steinhaus, *Toward matter dynamics in spin foam quantum gravity*, *Phys. Rev. D* **106** (2022) 106016 [[2206.04076](#)].
- [61] M. Han and H. Liu, *Analytic continuation of spinfoam models*, *Phys. Rev. D* **105** (2022) 024012 [[2104.06902](#)].
- [62] P. Donà, F. Gozzini and A. Nicotra, *Wick rotation for spin foam quantum gravity*, *Phys. Rev. D* **104** (2021) 126008 [[2106.14672](#)].
- [63] J. Ambjorn, A. Görlich, J. Jurkiewicz and R. Loll, *Nonperturbative quantum gravity*, *Phys. Rept.* **519** (2012) 127 [[1203.3591](#)].
- [64] S. Surya, *The causal set approach to quantum gravity*, *Living Rev. Rel.* **22** (2019) 5 [[1903.11544](#)].
- [65] P. Carlip, S. Carlip and S. Surya, *Path integral suppression of badly behaved causal sets*, *Class. Quant. Grav.* **40** (2023) 095004 [[2209.00327](#)].
- [66] M. Han, Z. Huang, H. Liu, D. Qu and Y. Wan, *Spinfoam on a Lefschetz thimble: Markov chain Monte Carlo computation of a Lorentzian spinfoam propagator*, *Phys. Rev. D* **103** (2021) 084026 [[2012.11515](#)].
- [67] J.W. Barrett, W.J. Fairbairn and F. Hellmann, *Quantum gravity asymptotics from the $SU(2)$ 15j symbol*, *Int. J. Mod. Phys. A* **25** (2010) 2897 [[0912.4907](#)].
- [68] M. Levin and C.P. Nave, *Tensor renormalization group approach to 2d classical lattice models*, *Phys. Rev. Lett.* **99** (2007) 120601 [[cond-mat/0611687](#)].
- [69] Z.-C. Gu and X.-G. Wen, *Tensor-Entanglement-Filtering Renormalization Approach and Symmetry Protected Topological Order*, *Phys. Rev. B* **80** (2009) 155131 [[0903.1069](#)].
- [70] G. Evenbly and G. Vidal, *Tensor network renormalization*, *Phys. Rev. Lett.* **115** (2015) 180405.
- [71] C. Delcamp and A. Tilloy, *Computing the renormalization group flow of two-dimensional ϕ^4 theory with tensor networks*, *Phys. Rev. Res.* **2** (2020) 033278 [[2003.12993](#)].
- [72] Y. Ito, D. Kadoh and Y. Sato, *Tensor network approach to 2D Lorentzian quantum Regge calculus*, *Phys. Rev. D* **106** (2022) 106004 [[2208.01571](#)].
- [73] B. Dittrich, F.C. Eckert and M. Martin-Benito, *Coarse graining methods for spin net and spin foam models*, *New J. Phys.* **14** (2012) 035008 [[1109.4927](#)].
- [74] B. Dittrich, M. Martin-Benito and E. Schnetter, *Coarse graining of spin net models: dynamics of intertwiners*, *New J. Phys.* **15** (2013) 103004 [[1306.2987](#)].
- [75] B. Dittrich, M. Martin-Benito and S. Steinhaus, *Quantum group spin nets: refinement limit and relation to spin foams*, *Phys. Rev. D* **90** (2014) 024058 [[1312.0905](#)].

- [76] B. Dittrich, E. Schnetter, C.J. Seth and S. Steinhaus, *Coarse graining flow of spin foam intertwiners*, *Phys. Rev. D* **94** (2016) 124050 [[1609.02429](#)].
- [77] S. Steinhaus, *Coupled intertwiner dynamics: A toy model for coupling matter to spin foam models*, *Phys. Rev. D* **92** (2015) 064007 [[1506.04749](#)].
- [78] B. Dittrich, S. Mizera and S. Steinhaus, *Decorated tensor network renormalization for lattice gauge theories and spin foam models*, *New J. Phys.* **18** (2016) 053009 [[1409.2407](#)].
- [79] C. Delcamp and B. Dittrich, *Towards a phase diagram for spin foams*, *Class. Quant. Grav.* **34** (2017) 225006 [[1612.04506](#)].
- [80] W.J. Cunningham, B. Dittrich and S. Steinhaus, *Tensor Network Renormalization with Fusion Charges—Applications to 3D Lattice Gauge Theory*, *Universe* **6** (2020) 97 [[2002.10472](#)].
- [81] B. Dittrich and M. Geiller, *Quantum gravity kinematics from extended TQFTs*, *New J. Phys.* **19** (2017) 013003 [[1604.05195](#)].
- [82] C. Delcamp, B. Dittrich and A. Riello, *Fusion basis for lattice gauge theory and loop quantum gravity*, *JHEP* **02** (2017) 061 [[1607.08881](#)].
- [83] A. Perelomov, *Generalized coherent states and their applications*, Springer, Berlin (1986).
- [84] T. Hahn, *The CUBA library*, *Nucl. Instrum. Meth.* **A559** (2006) 273 [[hep-ph/0509016](#)].
- [85] C. Allen, F. Girelli and S. Steinhaus, *Numerical evaluation of spin foam amplitudes beyond simplices*, *Phys. Rev. D* **105** (2022) 066003 [[2201.09902](#)].
- [86] N. Metropolis and S. Ulam, *The monte carlo method*, *Journal of the American Statistical Association* **44** (1949) 335.
- [87] W.K. Hastings, *Monte carlo sampling methods using markov chains and their applications*, *Biometrika* **57** (1970) 97.
- [88] B. Bahr and S. Steinhaus, *Investigation of the Spinfoam Path integral with Quantum Cuboid Intertwiners*, *Phys. Rev. D* **93** (2016) 104029 [[1508.07961](#)].
- [89] S. Chandrasekharan and U.-J. Wiese, *Meron cluster solution of a fermion sign problem*, *Phys. Rev. Lett.* **83** (1999) 3116 [[cond-mat/9902128](#)].
- [90] T.D. Kieu and C.J. Griffin, *Monte Carlo simulations with indefinite and complex valued measures*, *Phys. Rev. E* **49** (1994) 3855 [[hep-lat/9311072](#)].
- [91] S. Speziale, *Boosting Wigner’s nj-symbols*, *J. Math. Phys.* **58** (2017) 032501 [[1609.01632](#)].
- [92] S.K. Asante and T. Brysiewicz, *Solving the area-length systems in discrete gravity using homotopy continuation*, [2402.17080](#).
- [93] S.K. Asante, B. Dittrich and J. Padua-Arguelles, *Effective spin foam models for Lorentzian quantum gravity*, *Class. Quant. Grav.* **38** (2021) 195002 [[2104.00485](#)].